



**NTNU – Trondheim**  
Norwegian University of  
Science and Technology

# Effects of Potassium and Copper Promoters on Iron Fischer-Tropsch Catalysts

**Nils-Olav Andersen Hole**

Chemical Engineering and Biotechnology

Submission date: June 2015

Supervisor: Hilde Johnsen Venvik, IKP

Co-supervisor: Anders Holmen, IKP  
Rune Myrstad, SINTEF  
Jia Yang, SINTEF

Norwegian University of Science and Technology  
Department of Chemical Engineering



*"A scientist must be absolutely like a child. If he sees a thing, he must say that he sees it, whether it was what he thought he was going to see or not."*

- Douglas Adams



---

## Preface

This thesis is part of the Masters course TKP4900 Chemical Process Technology at the Department of Chemical Process Engineering, at the Norwegian University of Science and Technology (NTNU) in Trondheim. The work covering this thesis was conducted during a period of 20 weeks in the spring of 2015, in collaboration with SINTEF Materials and Chemistry.

The Fischer-Tropsch experiments were originally intended to be performed in a microstructured reactor, but due to time limitations and uncertainties in how the catalyst would behave in the reactor, a fixed-bed reactor was used instead. The microstructured reactor had not been tested with catalysts made from iron before, and there were certain worries the catalysts would lead to clogging of the microchannels. This could have had grave consequences for the restoration of the reactor, so it was decided to run several tests in the fixed-bed reactor first. In the end there was not enough time to start catalyst testing in the microreactor.

Trondheim, June 25<sup>th</sup> 2015

---

Nils-Olav Hole



---

## Acknowledgment

I would like to thank my supervisor Professor Hilde Venvik for her help during the course of the project, my co-supervisors, Professor Emeritus Anders Holmen for his suggestions and his positive feedback, and Research scientist Jia Yang for her contributions during my specialization project. I would especially thank Research scientist at SINTEF Rune Myrstad, for all his weeks of training and guidance in the use of the Fischer-Tropsch rig.

I would also thank my parents and my sister for their support, especially during these last five years, and for always showing admiration of my accomplishments.

Lastly, I would like to thank Dag Loe for our refreshing conversations during the work of my thesis, and Kristian Kvamsøe for comic relief and editing my thesis language. Thanks to them there hardly were any dull moments.

N.O.H.





---

## Abstract

The demand for energy is an ever increasing problem in the world today. The need for more abundant energy sources to take over the role of crude oil is becoming more and more present. GTL processes (gas-to-liquid), which utilizes the natural gas resources, are interesting replacements for the production of fuels in the future. One GTL process, the Fischer-Tropsch synthesis (FTS), produces fuel precursors by reacting a gaseous stream consisting of carbon monoxide and hydrogen.

The objective in this thesis was the fabrication of iron catalysts to enhance the production of desired products of the Fischer-Tropsch synthesis. Products like long chained hydrocarbons and olefins are desired, because they can later be refined into fuels like petrol and diesel. The effects of different promoter materials were studied, and it was decided to prepare the iron catalysts with small amounts of potassium and copper. All catalysts were prepared using the incipient wetness method with alumina support. In addition to testing the catalysts in a Fischer-Tropsch rig, the catalysts were also characterized using CO chemisorption and physisorption.

Some of the catalysts did not disperse the iron well on the support surface. This could indicate the metal piling up in multiple layers on the surface. One reason for this could be the method of preparation, with drying and calcining after each impregnation step.

Potassium proved to be the promoter material with largest implications regarding selectivity towards long chained hydrocarbons and olefins. Copper was originally added to yield higher activities and conversion rates for the catalysts, but these effects did not show for the experiments. It was instead another factor, namely a higher amount of iron in the catalysts, which proved to have the greatest impact on conversion rates.

Most of the catalysts run in the Fischer-Tropsch rig were activated with hydrogen at high temperatures. Two catalysts were in addition activated with synthesis gas, and though they had high selectivities towards olefins, these came at very low activities.



---

## Samandrag

Etterspurnaden for energi er eit stadig aukande problem i verda idag. Trongen for meir ressursrike energikjelder til å overta rolla til råolje vert meir og meir aktuelt. GTL-prosessar (gass til væske), som utnyttar naturgassressursane, er interessante erstatningar for å lage drivstoff i framtida. Éin GTL prosess, Fischer-Tropsch syntesa (FTS), produserar drivstoff ved å reagere ein gasstraum som er samansett av karbonmonoksid og hydrogen.

Målet med denne oppgåva var å lage jarnkatalysatorar for å auke produksjonen av ynskja produkt frå Fischer-Tropsch syntesa. Produkt som lange hydrokarbon og olefinar er ynskja, sidan dei seinare kan bli raffinert til drivstoff som bensin og diesel. Effekta av ulike promotormaterial vart studert, og det vart vedtatt å framstille jarnkatalysatorane med små mengder kalium og kopar. Alle katalysatorane vart framstilt ved å fuktimpregnere dei på bærarar av aluminiumoksid. I tillegg til å teste katalysatorane i ein Fischer-Tropsch rigg, vart dei òg karakterisert ved CO kjemisorpsjon og fysisorpsjon.

Nokre av katalysatorane spreidde ikkje jarnet godt på bæraroverflata. Dette kan indikere at metalla la seg i fleire lag på overflata. Ein av grunnane til dette kan vere framstillingsmetoden, med turking og kalsinering etter kvart impregneringssteg.

Kalium viste seg å vere det promotormaterialet med størst verknad på selektivitet av lange hydrokarbon og olefinar. Kopar vart opphaveleg lagt på for å gje høge aktivitetsmålningar og omsetnadsrater for katalysatorane, men dette var ikkje tilfellet for desse eksperimenta. Istadanfor var det ein annan faktor, nemleg ein høgare andel jarn i katalysatorane, som viste seg å ha den største påverknaden for omsetnadsratene.

Dei fleste katalysatorane som vart testa i Fischer-Tropsch riggen vart aktiverte med hydrogen ved høge temperaturar. To av katalysatorane vart i tillegg aktivert med syntesegass, og sjølv om dei viste høge selektivitetstal for olefinar, var aktivitetsmålningane altfor låge.



# Contents

Preface . . . . .	iii
Acknowledgment . . . . .	v
Abstract . . . . .	vii
Samandrag . . . . .	ix
<b>1 Introduction</b>	<b>1</b>
1.1 Approach . . . . .	2
1.2 Structure of the thesis . . . . .	2
<b>2 Theory</b>	<b>3</b>
2.1 Fischer-Tropsch synthesis . . . . .	3
2.1.1 Brief history . . . . .	3
2.1.2 Reactions and thermodynamics . . . . .	4
2.1.3 Reaction mechanism . . . . .	5
2.2 Catalysts . . . . .	8
2.2.1 Choice of catalyst . . . . .	9
2.3 Preparation of catalysts . . . . .	13
2.3.1 Incipient wetness method . . . . .	13
2.3.2 Drying and calcination . . . . .	13
2.3.3 Activation . . . . .	13
2.4 Catalyst characterization . . . . .	14
2.4.1 Chemisorption . . . . .	14
2.4.2 Physisorption . . . . .	15
2.5 Activity and selectivity measurements . . . . .	16
<b>3 Experimental</b>	<b>19</b>
3.1 Risk evaluation . . . . .	19
3.2 Catalyst preparation . . . . .	20

## CONTENTS

---

3.3	Catalyst characterization . . . . .	21
3.3.1	Chemisorption . . . . .	21
3.3.2	Physisorption . . . . .	21
3.4	Activity and selectivity measurements . . . . .	21
<b>4</b>	<b>Results</b>	<b>23</b>
4.1	Catalyst characterization . . . . .	23
4.1.1	Chemisorption . . . . .	23
4.1.2	Physisorption . . . . .	24
4.2	Activity and selectivity measurements . . . . .	24
4.2.1	Iron catalyst . . . . .	24
4.2.2	Potassium promoted catalysts . . . . .	27
4.2.3	Copper promoted catalysts . . . . .	31
4.2.4	Effects of syngas reduction . . . . .	34
4.2.5	CO <sub>2</sub> selectivity . . . . .	39
<b>5</b>	<b>Discussion</b>	<b>41</b>
5.1	Catalyst preparation . . . . .	41
5.1.1	Choice of catalyst promoters . . . . .	41
5.1.2	Incipient wetness method . . . . .	42
5.2	Catalyst characterization . . . . .	43
5.2.1	Chemisorption . . . . .	43
5.2.2	Physisorption . . . . .	43
5.3	Activity and selectivity measurements . . . . .	44
5.3.1	Activity . . . . .	44
5.3.2	Selectivity . . . . .	45
5.3.3	Olefin/paraffin ratios . . . . .	45
5.3.4	Hydrogen and syngas activation . . . . .	46
5.3.5	CO <sub>2</sub> production . . . . .	47
<b>6</b>	<b>Conclusions</b>	<b>49</b>
6.1	Summary and conclusions . . . . .	49
6.2	Recommendations for further work . . . . .	50
	<b>Bibliography</b>	<b>51</b>
<b>A</b>	<b>Risk assessment</b>	<b>I</b>

<b>B</b>	<b>Process flow diagram of the Fischer-Tropsch reactor system</b>	<b>IX</b>
<b>C</b>	<b>Chemical calculations for catalyst preparations</b>	<b>XI</b>
C.1	Amount of chemicals required for preparation of $20\text{Fe}_2\text{Cu}_5\text{K}$ . . . . .	XI
<b>D</b>	<b>Reproduced activity and selectivity measurements</b>	<b>XV</b>





# Acronyms

**20Fe** 20 wt% iron catalyst on Al<sub>2</sub>O<sub>3</sub> support

**20Fe1K** 20 wt% iron catalyst w/ K/Fe ratio of 1% on Al<sub>2</sub>O<sub>3</sub> support

**20Fe5K** 20 wt% iron catalyst w/ K/Fe ratio of 5% on Al<sub>2</sub>O<sub>3</sub> support

**20Fe2Cu5K** 20 wt% iron catalyst w/ Cu/Fe ratio of 2%, K/Fe ratio of 5% on Al<sub>2</sub>O<sub>3</sub> support

**30Fe2Cu5K** 30 wt% iron catalyst w/ Cu/Fe ratio of 2%, K/Fe ratio of 5% on Al<sub>2</sub>O<sub>3</sub> support

**BET** Brunauer-Emmett-Teller

**BJH** Barrett-Joyner-Halenda

**HC** Hydrocarbons

**FTS** Fischer-Tropsch synthesis

**GC** Gas chromatograph

**GHSV** Gas hourly space velocity

**GTL** Gas-to-liquid

**IWP** Incipient wetness point

**o/p** Olefin/Paraffin

**SG** Synthesis gas

**STY** Site time yield

**TOF** Turn-over frequency

**ToS** Time on stream

**WGS** Water Gas Shift



# List of symbols

$\alpha$	Probability of chain growth	-
$\theta$	Contact angle	°
$\sigma$	Surface tension	N/m
$\chi_{met}$	Weight fraction of active metal	%
$\omega_m$	Weight fraction of metal	%
$C$	BET constant	-
$D$	Metal dispersion	%
$F$	Adsorption stoichiometry factor	-
$n$	Number of moles	mol
$N_A$	Avogadro's number	mol <sup>-1</sup>
$n_{ads}$	Moles of substance adsorbed on a catalyst	mol/g
$m_{cat}$	Mass of catalyst	g
$M_{met}$	Molecular weight of metal	g/mol
$P$	Pressure	bar
$P_0$	Equilibrium pressure	bar
$r$	Pore radius	m
$R$	Gas constant	J/K mol
$r_{CO}$	Reaction rate of CO	mol/g <sub>cat</sub> h
$S_n$	Selectivity of n	%
$S_p$	Specific surface area	m <sup>2</sup> /g
$STY$	Site time yield	s <sup>-1</sup>
$T$	Temperature	K
$TOF$	Turn-over frequency	s <sup>-1</sup>
$V_0$	Volume occupied by one monolayer	mm <sup>3</sup>
$V_a$	Volume occupied by adsorbed molecule	mm <sup>3</sup>
$V_m$	Volume of one mole ideal gas	m <sup>3</sup> /mol



# List of Figures

2.1	Chain growth mechanism for Fischer-Tropsch synthesis . . . . .	6
2.2	Hydrocarbon fractions in the Fischer-Tropsch synthesis as a function of chain growth probability, $\alpha$ . . . . .	8
4.1	Activity and selectivity plots of the 20Fe catalyst at 20 bar and 230 °C reduced with hydrogen . . . . .	26
4.2	Activity and selectivity plots of the 20Fe1K catalyst at 20 bar and 230 °C reduced with hydrogen . . . . .	28
4.3	Activity and selectivity plots of the 20Fe5K catalyst at 20 bar and 230 °C reduced with hydrogen . . . . .	29
4.4	Activity and selectivity plots of the 20Fe2Cu5K catalyst at 20 bar and 230 °C reduced with hydrogen . . . . .	32
4.5	Activity and selectivity plots of the 30Fe2Cu5K catalyst at 20 bar and 230 °C reduced with hydrogen . . . . .	33
4.6	Activity and selectivity plots of the 20Fe5K catalyst at 20 bar and 230 °C reduced with syngas . . . . .	36
4.7	Activity and selectivity plots of the 20Fe2Cu5K catalyst at 20 bar and 230 °C reduced with syngas . . . . .	37
B.1	Flow diagram of the Fischer-Tropsch rig used for the activity and selectivity measurements. Adopted from Myrstad. . . . .	X
D.1	Activity and selectivity plots of reproduced experiments of the 20Fe5K catalyst at 20 bar and 230 °C reduced with hydrogen . . . . .	XVI
D.2	Activity and selectivity plots of reproduced experiments of the 20Fe2Cu5K catalyst at 20 bar and 230 °C reduced with hydrogen . . . . .	XVII
D.3	Activity and selectivity plots of reproduced experiments of the 20Fe5K catalyst at 20 bar and 230 °C reduced with syngas . . . . .	XVIII

D.4 Activity and selectivity plots of reproduced experiments of the 20Fe2Cu5K catalyst at 20 bar and 230 °C reduced with syngas . . . . . XIX

# List of Tables

2.1	World reserves of petroleum, natural gas and coal in 2011 <sup>[1][2][3]</sup> . . . . .	4
2.2	Properties of different support materials for iron without promoters <sup>[4]</sup> . . . . .	10
2.3	Properties of different support materials for iron with copper and potassium promoters <sup>[4]</sup> . . . . .	10
2.4	Properties of different support materials for iron with copper and potassium promoters <sup>[4]</sup> . . . . .	10
2.5	Effects of potassium and copper on an Fe <sub>2</sub> O <sub>3</sub> Zn catalyst <sup>[5]</sup> . . . . .	11
2.6	Effects of potassium, copper and SiO <sub>2</sub> on an iron catalyst <sup>[6]</sup> . . . . .	12
2.7	Effects of zinc on an Fe <sub>2</sub> O <sub>3</sub> KCu catalyst . . . . .	12
4.1	Metal dispersions and surface area of the five iron catalysts . . . . .	23
4.2	Surface area and pore volume of alumina support and iron catalysts with and without promoter . . . . .	24
4.3	Activity of the catalysts 20Fe, 20Fe1K and 20Fe5K at 20 bar and 230 °C at initial and steady-state conditions. . . . .	27
4.4	CO <sub>2</sub> -free CH <sub>4</sub> , C <sub>2</sub> -C <sub>4</sub> and C <sub>5</sub> + selectivities for the three catalysts 20Fe, 20Fe1K and 20Fe5K at steady-state conditions and at approximately equal CO conversion levels of ~ 40%. . . . .	30
4.5	Olefin/paraffin ratio of C <sub>2</sub> -C <sub>6</sub> hydrocarbons for the catalysts 20Fe, 20Fe1K and 20Fe5K at steady-state conditions and at approximately equal CO conversion levels. . . . .	30
4.6	Activity of the catalysts 20Fe5K, 20Fe2Cu5K and 30Fe2Cu5K at 20 bar and 230 °C at initial and steady-state conditions. . . . .	31
4.7	CO <sub>2</sub> -free CH <sub>4</sub> , C <sub>2</sub> -C <sub>4</sub> and C <sub>5</sub> + selectivities for the three catalysts 20Fe5K, 20Fe2Cu5K and 30Fe2Cu5K at steady-state conditions and at approximately equal CO conversion levels of ~ 40%. . . . .	34

## LIST OF TABLES

---

4.8	Olefin/paraffin ratio of C <sub>2</sub> -C <sub>6</sub> hydrocarbons for the catalysts 20Fe5K, 20Fe2Cu5K and 30Fe2Cu5K at steady-state conditions and at approximately equal CO conversion levels. . . . .	34
4.9	Activity of the catalysts 20Fe5K and 20Fe2Cu5K at 20 bar and 230 °C at initial and steady-state conditions, reduced in hydrogen and synthesis gas. . . . .	35
4.10	CO <sub>2</sub> -free CH <sub>4</sub> , C <sub>2</sub> -C <sub>4</sub> and C <sub>5</sub> + selectivities for the two catalysts 20Fe5K and 20Fe2Cu5K at steady-state conditions and at approximately equal CO conversion levels of ~ 30%. . . . .	38
4.11	Olefin/paraffin ratio of C <sub>2</sub> -C <sub>6</sub> hydrocarbons for the catalysts 20Fe5K and 20Fe2Cu5K reduced in hydrogen and synthesis gas at steady-state conditions and at approximately equal CO conversion levels. . . . .	38
4.12	CO <sub>2</sub> selectivity for the five catalysts at steady-state conditions. . . . .	39
C.1	Molecular weights of the involving metals and their corresponding nitrates, as well as water. . . . .	XI
C.2	Weight fractions of the involving metals and water in the left column in the different nitrates in the top row. . . . .	XII



# Chapter 1

## Introduction

This project will focus on the fabrication and testing of iron catalysts to be used for the Fischer-Tropsch synthesis. The Fischer-Tropsch synthesis deals with the conversion of syngas into hydrocarbons of different lengths and varying ratios of olefins and paraffins. Syngas is a combination of carbon monoxide and hydrogen either made from natural gas, coal, or biomass, and is a competitor to crude oil as a basis for production of fuels. The process was developed nearly 90 years ago, but has in recent years seen renewed interest following the change in politics concerning more environment friendly fuel production. As the oil reserves thin out, a greater focus will lie on the production of fuels from more abundant sources like natural gas and coal. On this basis it is important to have good processes able to deal with this challenge, and much resources have already been invested in intensifying processes like the Fischer-Tropsch synthesis.

The objective of this project is to study the effects different materials have on the product distribution of the Fischer-Tropsch synthesis. The materials will be studied, comparing their effects on CO conversion, selectivity, and properties like surface area and dispersion. The iron catalysts will contain at least one alkali or transition metal in order to promote its functions. Following the choice of materials, a preparation method will be proposed and conducted in the laboratory. Chemisorption and physisorption techniques will be used for characterization, and the catalysts will be run in a pilot set-up for Fischer-Tropsch synthesis using a fixed-bed reactor.

To examine the properties of the catalysts the results from the reactions will be compared to each other as well as to previously published works regarding iron catalysts for Fischer-Tropsch synthesis. The effect of different metal loadings will be investigated on basis of conversion, selectivities and olefin content, as well as activity. Attempts will be made to study all results at appropriate CO conversion levels.

## **1.1 Approach**

The thesis was started by first looking at the current literature on iron catalysts for Fischer-Tropsch synthesis. The focus was on noticing which promoter materials were most frequently used, and recognizing their effects on important parameters for the FTS. The next step was to investigate the different methods for preparation of the catalysts and decide upon one method to be used for the preparation of all catalysts. The fabrication of the catalysts were conducted in the laboratory, using multiple steps to load the metals onto the support material, followed by other preparation steps. Lastly the catalysts were characterized and finally tested in the fixed-bed FT reactors.

## **1.2 Structure of the thesis**

The rest of the thesis is organized as follows. Chapter 2 gives an introduction to the theory of the Fischer-Tropsch synthesis, covering its history and chemical mechanisms. This chapter also includes a literature survey, reporting the findings in preparation methods for the catalysts. Chapter 3 conveys the experimental method, detailing the techniques used for preparation, characterization and the FTS measurements. The results are presented in Chapter 4, and they are discussed in Chapter 5. The thesis ends with the conclusion in Chapter 6, which also includes some suggestions for further work.

# Chapter 2

## Theory

### 2.1 Fischer-Tropsch synthesis

#### 2.1.1 Brief history

Fischer-Tropsch synthesis (FTS) has a history reaching back over 90 years to the early 1920s. The process was developed by Franz Fischer and Hans Tropsch at the *Kaiser-Wilhelm-Institut für Chemie* in Berlin (today the *Max-Planck-Institut für Chemie*) and deals with the synthesis of hydrocarbons from synthesis gas (carbon monoxide and hydrogen)<sup>[7][8]</sup>. The technology was soon commercialized, and by the start of the second world war a large part of the fuel produced in Germany came from the Fischer-Tropsch synthesis, mainly from coal. Many of the German Fischer-Tropsch plants were destroyed during the second world war in an effort to stop the Germans from producing enough fuel. After the war there was a great interest from many countries to build their own Fischer-Tropsch plants, but compared to the magnitude and availability of cheap arabic oil most projects utilizing the FTS technology were unprofitable. The only country which actually went through with its projects was South Africa - with its Sasol plants - due to South Africa having an abundance of inexpensive coal. In the 1970s the price of oil increased dramatically, first with an oil embargo which led to the first oil crisis in 1973, and later with a second oil crisis in 1979. In this period many were concerned about the future price of crude oil, and the fact that oil reserves may one day come to an end. After this a number of projects utilizing the Fischer-Tropsch technology emerged in the US, Japan, and Europe, based on coal derivatives.

Over 90 years later the technology still sees great interest, and much experimental work is done to increase the efficiency of the synthesis and to reduce its production costs. In later years the demand for environment friendly energy sources have grown with the awareness

of the consequences fossil fuels have on the environment. The FTS process has benefited from this change in policy, and it is now seen as an option for energy production once the reserves of oil have run out, and when possibly hydrogen technology will dominate the energy market. Many reserves of natural gas are located in places that make it difficult to economically transport the gas. These reserves could be converted into liquid hydrocarbons using FT technology, and then transported in ships back to land. The Arabian Gulf, with its vast reserves of natural gas and shrinking oil reserves, is an area with high potential for implementation of FT plants. This potential is also present in countries around the North Sea and in Alaska. Table 2.1 shows the sizes of the available reserves of petroleum, natural gas, and coal in the world as of 2011, and it shows the reserves of both coal and natural gas to be far larger than the oil reserves<sup>[1][2][3]</sup>.

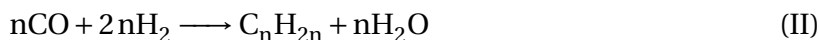
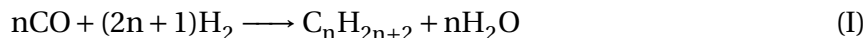
Table 2.1: World reserves of petroleum, natural gas and coal in 2011<sup>[1][2][3]</sup>

Energy reserves	Amount
Petroleum	1,473 billion barrels
Natural gas	1,194,746 billion barrels
Coal	888,851 million metric tons

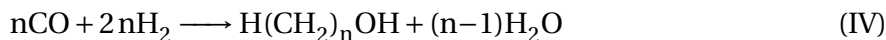
### 2.1.2 Reactions and thermodynamics

The Fischer-Tropsch synthesis uses syngas to mainly produce long-chained hydrocarbons, both paraffins and olefins, as shown in Reaction I and II respectively. However, there are some side reactions which produce a range of undesired products, among them the Boudouard reaction, Reaction V. In this reaction two CO molecules react and produce one CO<sub>2</sub> molecule. The production of alcohols is also an undesired reaction, as shown in Reaction IV.

Main reactions:



Side reactions:



The use of iron catalysts is preferred for synthesis gas derived from coal or biomass. This

is due to the low  $H_2/CO$  ratio ( $\sim 1$ ), which can be shifted using the water-gas shift reaction, as shown in Reaction III. Iron catalysts promote the shift in the direction of  $H_2$  production, effectively leading to a higher  $H_2/CO$  ratio in the reactor. Cobalt catalysts usually have little opposite effect on the water-gas shift reaction, shifting it slightly to the left and subsequently producing more CO at the expense of  $H_2$ . Thus cobalt catalysts are more suitable for reactions with syngas derived from natural gas<sup>[9]</sup>.

The reactions of the Fischer-Tropsch synthesis are characterized by their very high exothermicity, much higher than for the corresponding reactions in oil refining. Efficient heat removal is therefore of a major concern in the design of FT reactors, and many different reactors have been proposed for FTS. Fixed bed, slurry, and fluidized bed reactors are the most commonly used reactors in industry today<sup>[10]</sup>.

### 2.1.3 Reaction mechanism

The chemistry behind the Fischer-Tropsch synthesis is complex, and although several mechanisms have been proposed, it is still a lot of uncertainty connected with the understanding of the synthesis. Most commonly the FT mechanism is thought of as a one-carbon segment from a CO molecule connecting to an already existing hydrocarbon chain. In the next step the chain can either connect to another carbon segment and continue its propagation, or react with a hydrogen molecule and terminate. It is believed the probability for propagation,  $\alpha$ , and hence the corresponding probability for termination,  $1 - \alpha$ , is independent of chain length. In this way the product distribution can be represented as a simple statistical model, called the Anderson-Flory-Schulz (AFS) distribution. Figure 2.1 depicts the propagation and termination steps in the synthesis<sup>[7][11]</sup>.

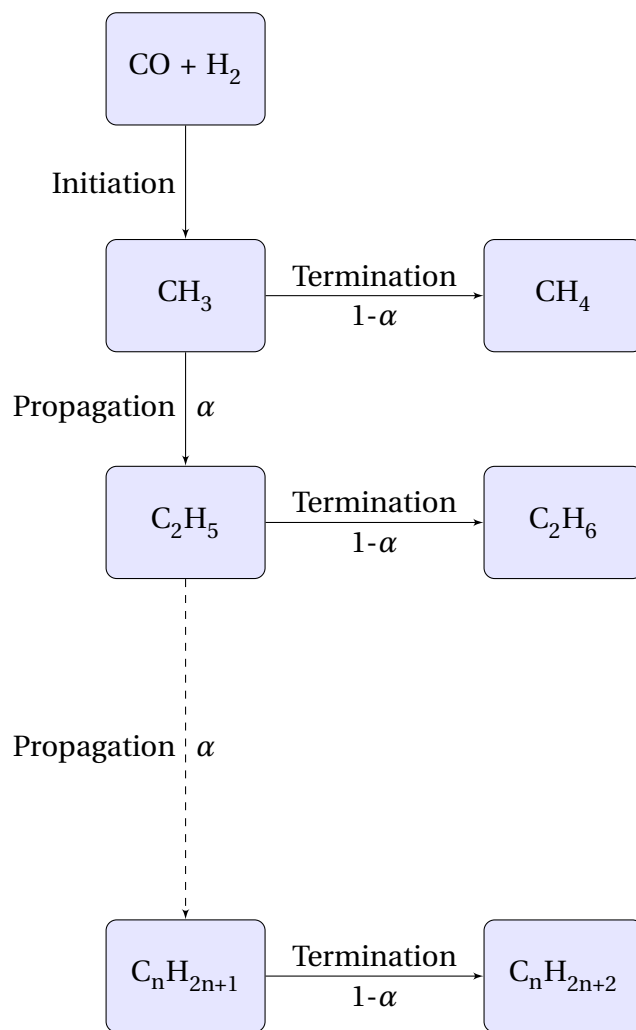


Figure 2.1: Chain growth mechanism for Fischer-Tropsch synthesis

There are several reaction steps connected to the attachment of one  $-\text{CH}_2-$  group to the hydrocarbon chain<sup>[7][11]</sup>:

- Associative adsorption of CO
- Splitting of the C–O bond
- Dissociative adsorption of  $2\text{H}_2$
- Transfer of  $\text{H}_2$  to make  $\text{H}_2\text{O}$
- Desorption of  $\text{H}_2\text{O}$
- Transfer of  $\text{H}_2$  to make a new  $-\text{CH}_2-$  group
- Formation of the new C–C bond

Among all the questions related to the order of these steps, one is particularly important:

- does the hydrogen attach itself to the CO group before the splitting of the C–O bond, leaving an oxygen containing intermediate
- or does the splitting occur first, yielding an intermediate group without oxygen?

Equation 2.1 is called the *Schulz-Flory*-equation for use in general polymerization reactions. Anderson was the one to see the uses for this in context with Fischer-Tropsch synthesis, and the one to further develop it to branching of methyl and ethyl. The product distribution from the Fischer-Tropsch synthesis can from Equation 2.1 be calculated as a function of chain-growth probability,  $\alpha$ . Figure 2.2 shows the result for some hydrocarbon fractions<sup>[8]</sup>.

$$\ln\left(\frac{S_n}{n}\right) = n \cdot \ln(\alpha) + \ln\left[\frac{(1-\alpha)^2}{\alpha}\right] \quad (2.1)$$

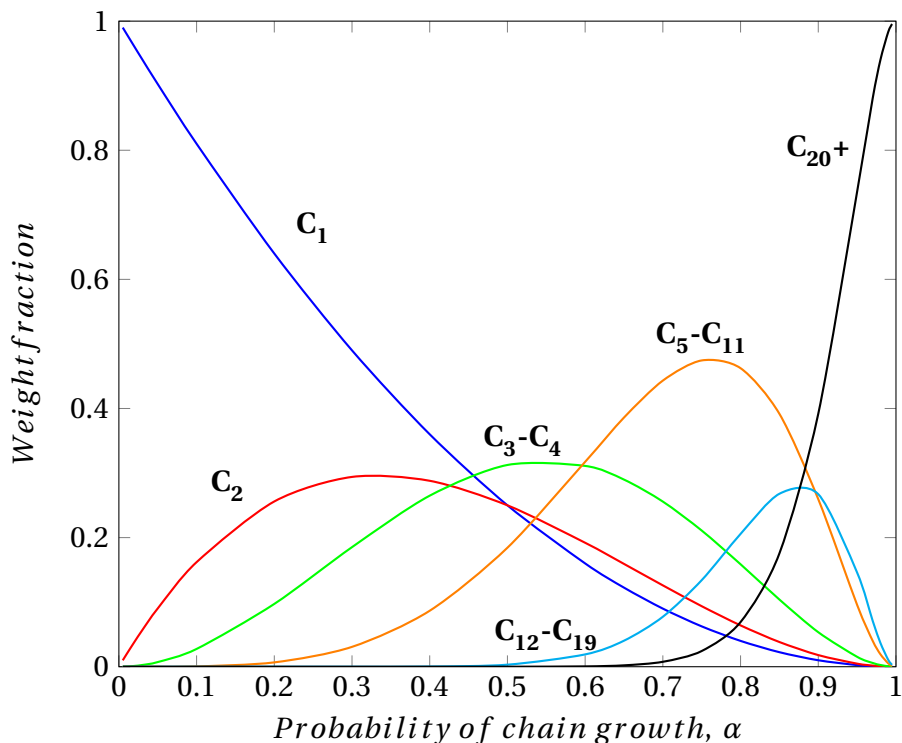


Figure 2.2: Hydrocarbon fractions in the Fischer-Tropsch synthesis as a function of chain growth probability,  $\alpha$

## 2.2 Catalysts

The Fischer-Tropsch synthesis produces hydrocarbons from a mixture of carbon monoxide and hydrogen, called synthesis gas, or syngas. Syngas is mainly produced from two sources, natural gas or coal. Depending on the source of syngas there will be different ratios of hydrogen and CO. Syngas from natural gas tends to have high hydrogen-to-CO ratios, while syngas produced from coal or biomass have low ratios. Either way the water gas shift reaction (WGS) as shown in Reaction III in Section 2.1.2 is required to shift the hydrogen and CO content to the desired ratio of  $\sim 2,1$ .

Cobalt catalysts are not active for WGS reaction, and are therefore best suited for hydrogen rich syngas derived from natural gas, while iron catalysts will drive the reaction to the right, and are best suited for CO-rich syngas derived from coal or biomass<sup>[12][13]</sup>. These are the two most commonly used catalysts for Fischer-Tropsch synthesis, and they were the first catalysts used by Franz Fischer and Hans Tropsch when they developed the technology in the 1920s. Nickel and ruthenium are also typical catalysts. Methane selectivity tends to increase at high temperatures when nickel is used as the catalyst, as opposed to the iron



catalyst which have low methane selectivities even at high temperatures. Ruthenium has been observed to be active at temperatures down to 150 °C, and with high molecular weight products. However, ruthenium catalysts are very expensive<sup>[7]</sup>.

The Fischer-Tropsch synthesis conditions are similar to the conditions allowing metals to form carbonyls, which suggests metal carbonyls on the surface will play an important role in the hydrocarbon formation<sup>[7][14]</sup>. The selected catalyst in this experiment is the iron catalyst, which gets activated after several iron carbide phases form in the initial stages of synthesis. Iron catalysts are flexible as they yield a wide range of products, from low molecular weight olefins to paraffin waxes. Sasol has developed several processes for the production of different products using iron as the catalyst. At temperatures of ~340 °C Sasol has managed to produce hydrocarbons with average molecular weights so low no liquid phase was even produced. The C<sub>3</sub> and C<sub>4</sub> olefins produced in this process are later oligomerized to be used as gasoline or as polymers in the chemical industry. In another process, low temperatures are used to keep the hydrocarbon products in liquid phase during reaction. A support material with wide pores is then used in order for the reactants to be able to fill the pores, and the product is later distilled to yield large fractions of waxes, as well as gasoline and diesel<sup>[12]</sup>.

### 2.2.1 Choice of catalyst

Promotion of the iron catalyst with alkali and transition metals is needed in order to obtain and retain high activities and stability over time. Potassium is widely used as a promoter to enhance conversion of CO and hydrogen, while other materials like copper, zinc and manganese have other advantages and can yield a different product range<sup>[5][9][13]</sup>.

#### Support material

Support materials will promote structural properties, so the choice of a good material is important for good stability<sup>[8]</sup>. Two alternatives were suggested for the iron catalyst, aluminium oxide (Al<sub>2</sub>O<sub>3</sub>) and silicon oxide (SiO<sub>2</sub>). Table 2.2 lists the general differences in surface area and pore volumes for the alumina and silica support. For both properties silica have the largest values, which means more active metals can be put on the silica support in monolayers compared to the alumina support. The larger pore volume also indicates longer chains and bigger networks of hydrocarbon product can be formed with the silica support<sup>[4][15]</sup>.

Table 2.2: Properties of different support materials for iron without promoters<sup>[4]</sup>

Support material	Silica	Alumina
Surface area [m <sup>2</sup> /g]	284	196
Pore volume [cm <sup>3</sup> /g]	1.15	0.43

Surface area and pore volume will most often be reduced as the active metal and promoters are loaded onto the support. Table 2.3 shows how the silica and alumina support in Table 2.2 changes with addition of iron, potassium and copper in atomic ratios of 100/250, 8.1/250 and 6/250 respectively compared to support. Surface area for both silica and alumina have been more than halved compared to their initial values, and likewise for pore volumes. However, this could be due to the method of preparation.

Table 2.3: Properties of different support materials for iron with copper and potassium promoters<sup>[4]</sup>

Support material	Silica	Alumina
Surface area [m <sup>2</sup> /g]	127	78
Pore volume [cm <sup>3</sup> /g]	0.53	0.19

However, a large surface area is not always equivalent with large conversions and selectivities of desired products. Table 2.4 lists conversion of CO both at its maximum and after 300 hours on stream, as well as the selectivity for methane production for the same catalysts used in Table 2.3. What is worth mentioning is even though silica have larger surface area than alumina, it has a smaller maximum conversion of CO, and also a greater loss of activity. The alumina catalyst had an induction period where the conversion increased from 40% to 60%, but it still managed to keep a high rate of conversion longer than the silica catalyst. The alumina catalyst also had a lower selectivity for methane. On the basis of these and other similar results, it was decided to use alumina as the support material.

Table 2.4: Properties of different support materials for iron with copper and potassium promoters<sup>[4]</sup>

Support material	Silica	Alumina
Maximum CO conversion [%]	32	63
CO conversion after 300 h [%]	25	62
CH <sub>4</sub> selectivity [%]	7-11	4-6

## Promoters

It is the general perception that promoter materials are required in order to make good iron catalysts. Several articles list many different types of materials, from alkali metals like potassium and sodium, via transition metals like zinc and manganese, to semi-metals like silicon. Some of the more common promoters will be presented here, and be compared on the basis of properties like conversion and selectivities.

Results from Iglesia et. al.<sup>[5]</sup> in Table 2.5 show how varying loads of potassium and copper on an iron oxide-zinc catalyst affect the conversion of CO, the selectivity of methane production, and also a relation between 1-pentene and n-pentane to represent the relation between olefin and paraffin production. The table shows how the conversion of CO increases, both for additions of potassium and copper, and in particular when both are present on the same catalyst. The selectivity towards methane increases with the addition of copper, as the selectivity goes from 4.8% to 10.2% when the catalyst contains a small amount of copper. Using a catalyst with some potassium seems to have the opposite effect, as the selectivity for methane is reduced from 4.8% to 1.8%. However, too much potassium promoter apparently vanes the effect, as more methane is produced with the 0.04K, 0.01Cu catalyst than with the 0.02K, 0.01Cu catalyst. The relation between olefin and paraffin production is relatively unaffected by the different promoter loadings, even though a little more olefines is produced with potassium as the promoter, and copper may enhance the production of paraffines. Previous literature supports the positive effects of potassium on iron catalysts, but only to a certain degree. The effects are evident up to a ratio of  $\sim 5/100$  potassium atom per iron atom. Above this ratio the results will no longer show any significant improvement<sup>[16]</sup>.

Table 2.5: Effects of potassium and copper on an  $\text{Fe}_2\text{O}_3\text{Zn}$  catalyst<sup>[5]</sup>

K/Fe ratio	Cu/Fe ratio	CO conv. [CO/h g Fe]	CH <sub>4</sub> sel.	Olefin/Paraffin ratio
0	0	0.70	4.8%	1.9
0	0.01	0.87	10.2%	1.7
0.02	0	1.23	1.8%	1.8
0.02	0.01	2.40	1.8%	1.8
0.02	0.02	2.43	2.0%	1.8
0.04	0.01	2.49	2.5%	2.0

In Table 2.6, Hayakawa et. al.<sup>[6]</sup> again shows how CO conversion changes with potas-

sium and copper, , with the addition of one data point for silicon oxide. The table shows the selectivity of hydrocarbon chains containing 5 carbon atoms or longer. As in Table 2.5 the conversion increases with promoter, especially when both potassium and copper are present. Silicon oxide does not have the similar positive effects on the conversion level as potassium, but it will affect the selectivity towards production of long chained hydrocarbons, at least more than what is recorded for potassium.

Table 2.6: Effects of potassium, copper and SiO<sub>2</sub> on an iron catalyst<sup>[6]</sup>

K/Fe ratio	Cu/Fe ratio	SiO <sub>2</sub> /Fe ratio	CO conversion	C <sub>5</sub> + selectivity
0	-	-	34.1%	53.5%
0.003	0.020	0.088	66.0%	73.5%
0.007	0.022		85.9%	70.3%
0.012	-	-	80.1 %	81.6%

Table 2.7 shows the effects zinc have on the properties of an iron oxide catalyst with potassium and copper promotion. The conversion of CO increases with amount of zinc on the catalyst, but unfortunately so does the methane selectivity. The largest increase in selectivity of methane occurs from a 0.1 load of zinc to a 0.4 load, while the largest increase in conversion occurs from 0 to 0.1 zinc load. By not applying too much zinc on the iron catalyst the problem with selectivity towards methane could be avoided, and at the same time still obtain a fairly high conversion. A relation between zinc load and the ratio of olefin and paraffin is not clear from these results<sup>[17]</sup>.

Table 2.7: Effects of zinc on an Fe<sub>2</sub>O<sub>3</sub>KCu catalyst

Zn/Fe ratio	CO conversion [CO/h g Fe]	CH <sub>4</sub> selectivity	Olefin/Paraffin ratio
0	1.52	1.7%	1.9
0.1	2.4	1.8%	1.8
0.4	2.63	2.3%	2.0

From the results presented above, it is obvious the iron catalyst requires promoters in order to reach its full potential, and to increase its productivity towards desired products. Most sources mention potassium and copper as the most essential materials for promoting iron catalysts<sup>[18][9][4]</sup>.

## 2.3 Preparation of catalysts

All catalysts were prepared using the incipient wetness method, in some cases in multiple steps. After each step they were dried and calcined for an appropriate amount of time. Before they could be used in reactions they needed to be activated at high temperatures in the presence of either hydrogen or syngas.

### 2.3.1 Incipient wetness method

In the incipient wetness method the support material gets impregnated with an aqueous solution of the active metal salt. The solution must contain the correct concentration of the active metal in order for the finished catalyst to obtain the correct loading. A salt is solved in a calculated amount of deionized water to precisely fill up the pores of the supported material. The amount of water is found first by dripping water on the material until it is completely saturated. At this point, instead of water filling up the pores in the material, the material starts dissolving in the water. This is called the *incipient wetness point*. If the solubility is too low for the salt to be dissolved in the required amount of water, the impregnation of the metal needs to be done in several steps<sup>[19]</sup>.

### 2.3.2 Drying and calcination

After the impregnation of the metal, the solvent needs to be removed. This is done by drying the unfinished catalyst at low to medium temperatures until all the solvent has dried up<sup>[20]</sup>. Later on the catalyst precursor undergoes calcination. In this step the precursor is exposed to high temperatures with an air or nitrogen flow, often for many hours. Unwanted water and nitrates from the salt solution are removed in this process, and in addition the surface atoms get oxidized<sup>[21]</sup>.

### 2.3.3 Activation

The catalyst is activated by reduction in a reduction medium. Most Fischer-Tropsch experiments are activated by either hydrogen, a mixture of hydrogen and helium or syngas<sup>[22][23]</sup>. The iron oxide is reduced to iron as shown in Reaction VI.



The reaction temperature is important due to the formation of metal crystallites. The iron catalyst requires high temperatures over 400°C<sup>[8][24][25]</sup>.

## 2.4 Catalyst characterization

For this project the characterization techniques of chemisorption with CO and physisorption were conducted. In this section the two techniques are presented, with descriptions of how the activity calculations were performed.

### 2.4.1 Chemisorption

Chemisorption is a technique used for finding catalytic dispersion. Dispersion is defined as in Equation 2.2 as the number of metal atoms on the surface of a support per total number of atoms<sup>[19]</sup>.

$$D = \frac{\text{Number of surface metal atoms}}{\text{Total number of metal atoms}} \quad (2.2)$$

Usually, hydrogen, CO, or oxygen is actively chemisorbed on the surface of the catalyst metal atoms. CO is used for the chemisorption of iron catalysts, and it is assumed one CO molecule covers one iron site 1:1<sup>[8]</sup>.

Experiments were conducted by measuring the volume of CO adsorbed on the surface at increasing pressures and at constant temperature. The adsorption isotherm is then obtained by plotting the CO adsorbed against equilibrium pressure. Monolayer coverage is found by extrapolating the linear part of the isotherm to zero pressure. The dispersion value can then be calculated from Equation 2.3<sup>[8]</sup>.

$$D = \frac{n_{ads} \cdot M_m \cdot F}{\chi_{met}} \quad (2.3)$$

where

- D is the metal dispersion [%]
- $n_{ads}$  is the moles of gas adsorbed on the catalyst [mol/g<sub>cat</sub>]
- $M_{met}$  is the molecular weight of the active metal [g/mol]
- F is the adsorption stoichiometry factor
- $\chi_{met}$  is the weight fraction of active metal in the catalyst [%]

### 2.4.2 Physisorption

The BET (Brunauer-Emmett-Teller) method is a procedure based on adsorption of nitrogen at liquid temperatures<sup>[26]</sup>. Each nitrogen molecule occupies an area on the catalyst surface equal to its cross-sectional area. Since the area every nitrogen molecule occupies is known, it is possible to calculate the total surface area of the catalyst by counting the number of molecules adsorbed at monolayer coverage. The amount of nitrogen adsorbed on the surface is measured as a function of pressure, and can be expressed by Equation 2.4.

$$\frac{1}{V_a \cdot \left(\frac{P_0}{P} - 1\right)} = \frac{1}{V_0 \cdot C} + \frac{C-1}{V_0 \cdot C} \cdot \frac{P}{P_0} \quad (2.4)$$

where

- $V_a$  is the volume each adsorbed molecule occupies
- $P_0$  is the pressure at equilibrium [bar]
- $P$  is the pressure of the gas [bar]
- $V_0$  is the volume the first monolayer occupies
- $C$  is the BET constant, designed to account for the difference in energy between the first monolayer and the sequential layers

The equation can be rewritten as

$$\frac{1}{V_a \cdot \left(\frac{P_0}{P} - 1\right)} = s \cdot \frac{P}{P_0} + i \quad (2.5)$$

where  $s = \frac{C-1}{V_0 \cdot C}$ , and  $i = \frac{1}{V_0 \cdot C}$ . By plotting  $\frac{1}{V_a \cdot \left(\frac{P_0}{P} - 1\right)}$  as a function of  $\frac{P}{P_0}$ , a straight line will be obtained with slope  $s$  and intersection at  $i$ . An expression for the volume of the first monolayer,  $V_0$ , can be calculated by combining the expressions for  $s$  and  $i$ ,  $V_0 = \frac{1}{s+i}$ . The value of  $V_0$  is then calculated by inserting the values of  $s$  and  $i$  from the plot. The specific surface area can be calculated from Equation 2.6 by assuming standard temperature and pressure.

$$S_p = \frac{V_0 \cdot N_A \cdot A}{m_{cat} \cdot V_m} \quad (2.6)$$

where

- $N_A$  is Avogadro's number

- $A$  is area occupied by one molecule
- $m_{cat}$  is the mass of the catalyst
- $V_m$  is the volume of one mole ideal gas

To calculate the volume of the pores, the BJH (Barrett-Joyner-Halenda) method is used. The pores are filled with nitrogen at high relative pressures in order to condense  $N_2$  in the catalyst pores. The pores are then gradually emptied by decreasing the relative pressure. By using the Kelvin model, Equation 2.7, the pore volume and pore size can be calculated.

$$\ln\left(\frac{P}{P_0}\right) = -\frac{2 \cdot \sigma \cdot V \cdot \cos\theta}{r \cdot R \cdot T} \quad (2.7)$$

where

- $\sigma$  is the surface tension of liquid nitrogen
- $V$  is the molar volume of liquid nitrogen
- $\theta$  is the contact angle
- $r$  is the radius of the pore
- $R$  is the gas constant
- $T$  is the temperature

## 2.5 Activity and selectivity measurements

Fischer-Tropsch synthesis is conducted in a fixed-bed reactor. The reactor is part of a larger system made up of in total four fixed-bed reactors. A sketch of the system is pictured in Appendix B<sup>[27]</sup>. The reactor is constructed of steel, built to withstand acidic materials. It has an internal diameter of 1/4", and can be run at pressures up to 50 bar and temperatures up to 500 °C. The whole system is protected by a polycarbonate chamber connected to ventilation, and contains detectors for CO and H<sub>2</sub>. Syngas with a fixed ratio of CO and hydrogen is first run through a filter made of PbO to clean the gas for iron carbonyls, before being heated to the desired temperature and fed to the reactor inlet. The reactors are placed vertically so the product will leave the reactor from the bottom. Some of the product is led to a gas chromatograph which analyzes continually. The GC and corresponding FTS rig are



calibrated annually<sup>[28]</sup>.

The activity of the specific catalyst is measured by the Site Time Yield (STY). STY is defined as the number of moles produced of a desired product per active site on the catalyst surface per unit of time<sup>[29]</sup>. The STY is closely related to the turn-over frequency (TOF), which measures the number of moles reacted per site per time. The definition of STY is shown in Equation 2.8.

$$STY = \frac{r_{CO} \cdot M_m}{\omega_m \cdot D} \quad (2.8)$$

where

- $r_{CO}$  is the rate of reaction of CO [mol/g h]
- $M_m$  is the molecular weight [g/mol]
- $\omega_m$  is the weight fraction of metal in the catalyst [%]
- $D$  is the dispersion, as calculated from chemisorption [%]

From the chemisorption data the adsorption isotherm can be drawn. Assuming CO:Fe coverage of 1:1<sup>[8]</sup>, the dispersion is calculated using the ideal gas law as shown in Equation 2.9.

$$PV = nRT \quad (2.9)$$



# Chapter 3

## Experimental

The following chapter details the method of the experimental work. Firstly the steps in the preparation of the catalyst, followed by the method of characterization, and finally the experimental run in the fixed-bed reactor.

### 3.1 Risk evaluation

Before any work could be performed in the labs, a risk evaluation form was required to be filled out. The evaluation lists the dangers connected to experimental work, the risks of working with hazardous materials, as well as precautions taken beforehand. The NTNU HSE Handbook was used as basis for the risk evaluation, together with knowledge obtained during training for the instruments. In cases of uncertainty the instrument responsible was always contacted before any further action was taken.

The evaluation consisted of judging the likelihood of risks and potential consequences for some scenarios concerning the use of instruments. If some of the combined likelihoods and consequences were found to be too grave, solutions were proposed.

The risk evaluation form is attached in Appendix A.

## 3.2 Catalyst preparation

A total of five catalysts were prepared using the incipient wetness method as described in Section 2.3, all of which were supported with aluminum oxide. The catalysts consisted of

- 20 wt% iron on alumina support
- 20 wt% iron, and potassium with an atomic ratio of 1/100 relative to iron on alumina support
- 20 wt% iron, and potassium with an atomic ratio of 5/100 relative to iron on alumina support
- 20 wt% iron, copper with an atomic ratio of 2/100 relative to iron, and potassium with an atomic ratio of 5/100 relative to iron on alumina support
- 30 wt% iron, copper with an atomic ratio of 2/100 relative to iron, and potassium with an atomic ratio of 5/100 relative to iron on alumina support

For simplicity the catalysts were named 20Fe, 20Fe1K, 20Fe5K, 20Fe2Cu5K and 30Fe2Cu5K respectively to reflect their contents of active metals and promoters.

The preparation of the catalyst was started by measuring approximately 100 g of aluminium oxide and calcining it at 500 °C for 4 hours. The alumina, which was going to be used as support material for the catalyst, was then sieved to particle sizes of 53-90  $\mu\text{m}$ . The catalyst was prepared via the incipient wetness method using aqueous solutions of ferric nitrate. First the incipient wetness point was found. This was done by using deionized water, exactly approximately 10 g of support, and then calculating a value of g  $\text{H}_2\text{O}$ /g support. For the two catalysts containing copper, the copper was coimpregnated with iron, calculating the desired ratio between ferric and cupric nitrate. The ferric nitrate was added in two or three steps in order to reach the desired loading of 20 and 30 wt% iron respectively. After each step the sample was dried at 120 °C for 2 hours, and later calcined in flowing air at 300 °C for 16 hours with a heating rate of 4 °C/min. After all the iron and copper was added, the potassium promoter was attached to the catalyst. Aqueous potassium nitrate was impregnated in the same way as with the ferric nitrate. The catalysts with potassium promoter was dried at 120 °C for 2 hours, and calcined in air at 300 °C for 5 hours. After the impregnation was completed, the catalysts were sieved to particle sizes of 53-90  $\mu\text{m}$ .

### 3.3 Catalyst characterization

The catalysts were characterized by CO chemisorption and nitrogen physisorption, as presented in Section 3.3.1 and 3.3.2.

#### 3.3.1 Chemisorption

CO chemisorption was conducted in a Micromeritics ASAP 2020 system on catalysts of sample sizes of ~140 mg. Each sample was placed in a U-shaped reactor between two pieces of carefully placed quartz wool. Evacuation to approximate vacuum was followed by a subsequent leak test, where a leakage higher than 0.05 mmHg/min was not allowed. The samples were pretreated at 450 °C for 16 hours in flowing hydrogen with a temperature-programmed heating of 2 K/min<sup>[8]</sup>. After the reduction step, the samples were cooled to 100 °C using flowing helium followed by evacuation to  $<5 \cdot 10^{-5}$  mmHg and a subsequent cooling to 40 °C. The experiment was then conducted by exposing the sample to known amounts of CO and recording the increase in pressure.

#### 3.3.2 Physisorption

The Micromeritics TriStarII 3020 Surface Area and Porosity Analyzer was used for the physisorption measurements. Both of the measurements, surface area by the BET method, and the pore size distribution by the BJH method were conducted in this apparatus<sup>[26]</sup>. Approximately 140 mg sample sizes of each of the five catalysts, in addition to the pure alumina support, were tested. Prior to the measurements the samples were placed in a bulb reactor and degassed at 200 °C. After the pressures in the reactors passed below 100 mmHg, usually overnight, the reactors were placed in the ports of the apparatus and emerged in liquid nitrogen. After the analysis finished, the samples were weighted once more and the analysis files were corrected with any weight changes that occurred.

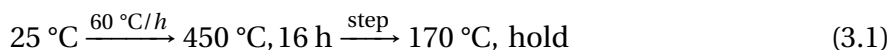
### 3.4 Activity and selectivity measurements

All experiments measuring the activities and selectivities of the catalysts were performed in any of the four parallel fixed bed Fischer-Tropsch reactors. The catalysts 20Fe, 20Fe1K and 30Fe2Cu5K were only tested once, while the catalysts 20Fe5K and 20Fe2Cu5K were tested for two runs. In addition, the same two catalysts, 20Fe5K and 20Fe2Cu5K, were tested with

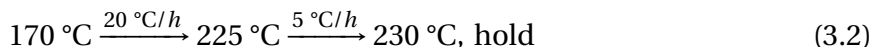
syngas instead of hydrogen in the activation step. The catalysts were suspected of deactivation due to a slightly uphold in the flow of syngas during activation, so the experiments were run once more for both catalysts.

About 2 grams of each catalyst was diluted with silicon carbide in a ratio of 2:19 in order to spread the heat developing during reaction, hence the reducing of the temperature gradients. The catalyst/silicon carbide mixture was placed in the reactor with a mesh in the bottom and quartz wool in both ends of the reactor. Very carefully, in order to prevent the catalysts from compressing to a solid mass, the reactors were installed in the reactor system. The reactors were placed in an oven with an aluminium jacket enclosing them, and a thermocouple was placed through the reactor bed. Afterward, the pressure in the reactors was slowly built up to about 18 bar, at which point hydrogen was added until a final pressure of 20 bar was achieved. The hydrogen was added to perform a leak test, after which all nuts and bolts were securely tightened.

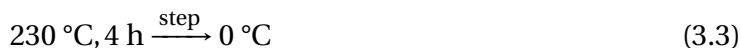
The catalysts were reduced in-situ at temperatures of 450 °C for 16 hours<sup>[8]</sup>, with an increase in temperature of 60 °C/h, as shown in Equation 3.1.



The reaction was started by changing the gas flow into the reactors to syngas with a H<sub>2</sub>/CO ratio of 2.1 at 20 bar and 170 °C. The temperature was then gradually increased until it reached 230°C, as shown in Equation 3.2.



After about 24 hours on stream the gas flow of the syngas was tweaked in an effort to reach a CO conversion of about 40-50%, a chosen level to compare the catalysts on. The product was removed every other day, as well as at the end of each experiment. After about 100 hours on stream the experiments were shut down. First the gas into the reactor was changed from syngas to helium in order to more easily remove the used catalyst from the reactor after the experiment. Then a temperature program consisting of cooling the reactors to room temperature was initiated, as shown in Equation 3.3.



# Chapter 4

## Results

The following section presents the results from physisorption, CO chemisorption, and the experiment conducted in the fixed-bed reactors. The results will be commented on and compared to other works in the discussion section, Section 5.

### 4.1 Catalyst characterization

#### 4.1.1 Chemisorption

Table 4.1 lists the dispersion of metal on the catalyst surface, as well as the area the metal occupies. The highest dispersion was obtained for the catalyst 20Fe5K, while the catalyst 30Fe2Cu5K displayed the lowest dispersion of all catalysts. There is no clear trend in the dispersion values, however it may be observed that the catalyst which required most impregnation steps also have the lowest dispersion.

Table 4.1: Metal dispersions and surface area of the five iron catalysts

Catalyst	Dispersion [%]	Metal surface area [m <sup>2</sup> /g]
20Fe	1.23	1.63
20Fe1K	0.51	0.67
20Fe5K	1.65	2.18
20Fe2Cu5K	0.98	1.33
30Fe2Cu5K	0.27	0.54

### 4.1.2 Physisorption

Table 4.2 shows the surface area and pore volumes of the six samples tested in the physisorption test. The physisorption was conducted in a Micromeritics Tristar II 3020 apparatus with flowing nitrogen. Surface area was calculated using BET method, while pore volume was calculated by the BJH method simultaneously. The characterization was done for both calcined alumina support, and the five iron catalysts.

Table 4.2: Surface area and pore volume of alumina support and iron catalysts with and without promoter

Sample	Surface area [m <sup>2</sup> /g]	Pore volume [cm <sup>3</sup> /g]
Alumina support	161.4	0.68
20Fe	128.5	0.45
20Fe1K	138.6	-
20Fe5K	123.9	0.43
20Fe2Cu5K	123.3	-
30Fe2Cu5K	108.0	-

## 4.2 Activity and selectivity measurements

This section presents the results from the activity and selectivity measurements. The results are divided into five sections. In Section 4.2.1 the results obtained using catalyst 20Fe without any promoters are presented. Section 4.2.2 presents the results from the experiments using the potassium promoted iron catalysts, 20Fe1K and 20Fe5K, and in Section 4.2.3 the results obtained using both potassium and copper promoted iron catalysts, 20Fe2Cu5K and 30Fe2Cu5K, are presented. The results in these first three sections were all obtained using catalysts activated in hydrogen. Section 4.2.4 shows the results from two experiments conducted by first activating the catalysts using synthesis gas, whereupon they were treated in the same way as the catalysts activated by hydrogen. Section 4.2.5 lists the selectivity towards CO<sub>2</sub> in all the experiments.

### 4.2.1 Iron catalyst

One experiment was conducted with catalyst 20Fe in order to compare the results to the ones obtained with catalysts containing promoter materials. The catalyst was reduced in hydrogen and reaction was started with a gas hourly space velocity (GHSV) of 7,508 Ncm<sup>3</sup>/g h.



The CO conversion only reached levels of approximately 14%, and the GHSV was subsequently lowered to 2,282 Ncm<sup>3</sup>/g h after about 24 hours on stream. The conversion level then increased to around 30%, and was allowed to stabilize for another 24 hours before the GHSV was further lowered, this time to 1,502 Ncm<sup>3</sup>/g h. At this value the catalyst showed stable conversion levels of CO slightly below 40%. The CO conversion is shown for catalyst 20Fe in Figure 4.1a.

Figure 4.1b shows the selectivities of CO<sub>2</sub>-free CH<sub>4</sub>, C<sub>2</sub>-C<sub>4</sub> and C<sub>5</sub>+ in the product stream. As the GHSV values decrease, i.e. the CO conversion increases, the selectivity of C<sub>5</sub>+ hydrocarbons decreases only slightly (5-6%). The production of hydrocarbons with medium chainlength C<sub>2</sub>-C<sub>4</sub> is increasing with the same 5-6% towards the end of the experiment. The methane selectivity is not affected as it stays the same throughout the whole experiment.

However, the CO<sub>2</sub> selectivity is not as stable. Shown in Figure 4.1d, it first increases from ~ 5% to 10% at the first adjustment of the GHSV, and later to 12-13% at the second adjustment. This correlates well with the CO conversion levels shown in Figure 4.1a. Both the CO<sub>2</sub> selectivity and the conversion of CO doubles as the GHSV goes from 7,508 to 2,282 Ncm<sup>3</sup>/g h, and both measurements increase to values approximately 30% higher than its previous values at the second adjustment of the GHSV.

The ratio between olefin and paraffin production for hydrocarbons with different chainlength is shown in Figure 4.1c. The figure shows the fraction of olefins decreasing for all lengths of hydrocarbons, although the ratio of propene/propane have the highest values regardless of conversion level, and the ethene/ethane ratio is the lowest measured.

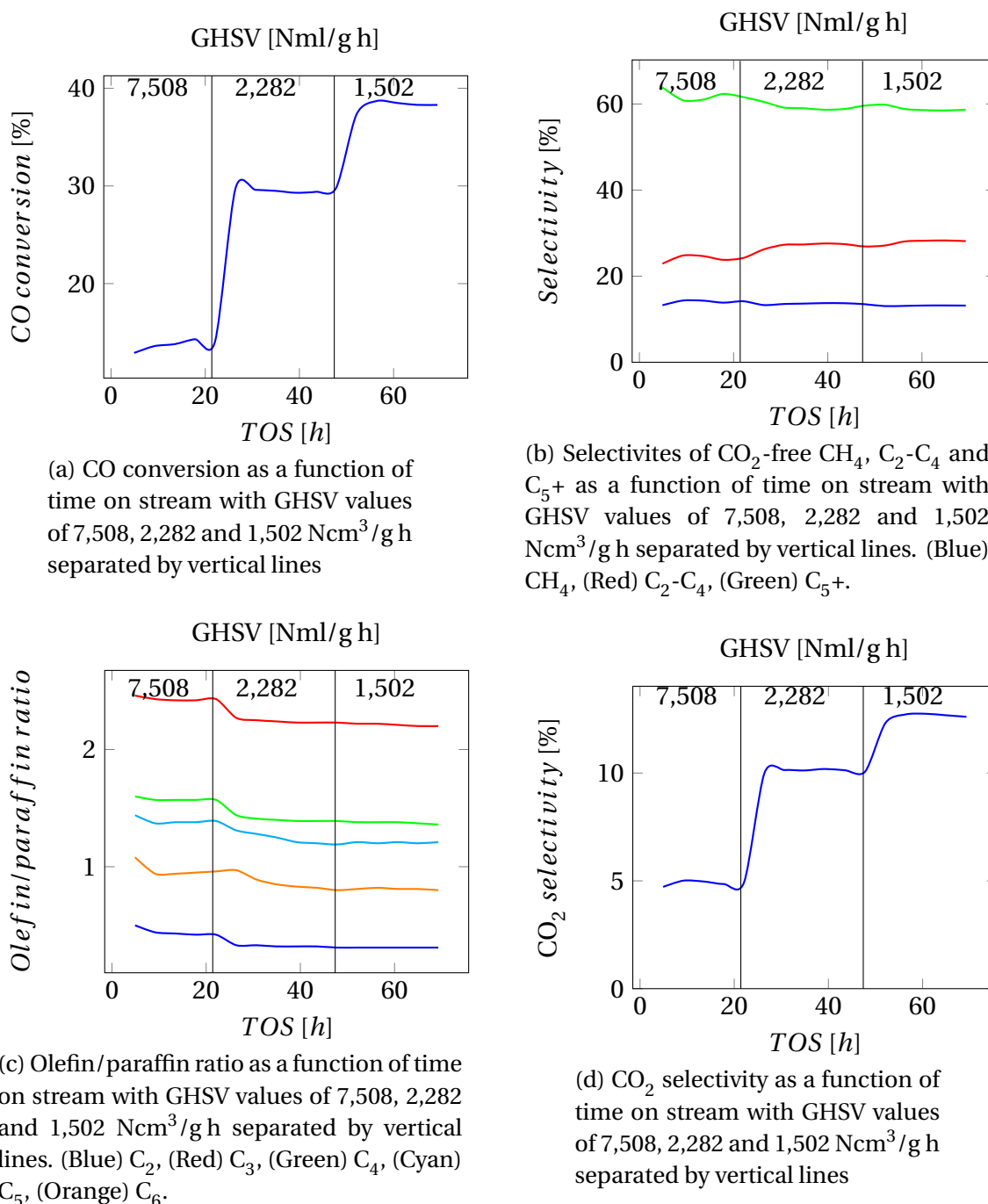


Figure 4.1: Activity and selectivity plots of the 20Fe catalyst at 20 bar and 230 °C reduced with hydrogen

## 4.2.2 Potassium promoted catalysts

Figures 4.2 and 4.3 shows the activity and selectivity measurements for the two catalysts 20Fe1K and 20Fe5K. The values are also listed in Tables 4.3, 4.4 and 4.5 at initial conditions and at steady-state conversion levels. The tables also compares selectivities, activity and olefin/paraffin ratios for the two catalysts with the values obtained with catalyst 20Fe, as reported in Section 4.2.1. From the figures it can be seen the CO conversion starts at about 15% for both catalysts, but both reach conversion levels of 40% after the space velocities are reduced to around 1,500 Ncm<sup>3</sup>/gh. However, the conversion for catalyst 20Fe5K suddenly dropped after reaching 40% conversion.

Figures 4.2b and 4.3b shows the C<sub>5</sub>+ selectivity decreasing slightly for the two catalysts as conversion increases, while C<sub>2</sub>-C<sub>4</sub> selectivity increases.

The conversion also affects the olefin/paraffin ratios negatively, as shown in Figures 4.2c and 4.3c. As for the catalyst 20Fe, the two potassium containing catalysts also obtained the highest olefin/paraffin ratios for C<sub>3</sub>, and lowest for C<sub>2</sub>.

20Fe5K has a higher selectivity towards CO<sub>2</sub> than 20Fe1K at both initial and steady-state levels, as shown in Figures 4.2d and 4.3d.

Table 4.3: Activity of the catalysts 20Fe, 20Fe1K and 20Fe5K at 20 bar and 230 °C at initial and steady-state conditions.

Catalyst	20Fe		20Fe1K		20Fe5K	
	I	SS	I	SS	I	SS
ToS [h]	22.1	69.3	52.8	92.5	25.0	59.7
GHSV [Ncm <sup>3</sup> /g h]	7,508	1,502	7,419	1,484	14,139	2,262
CO conversion [%]	14.1	38.3	14.8	37.9	11.7	41.0
r [mol CO/g h]	0.015	0.008	0.015	0.008	0.023	0.013
STY [s <sup>-1</sup> ]	0.096	0.052	0.241	0.123	0.112	0.063

Table 4.3 shows the 20Fe5K catalyst to reach CO conversions of ~ 40% at a much higher space velocity than for the 20Fe and 20Fe1K catalysts.

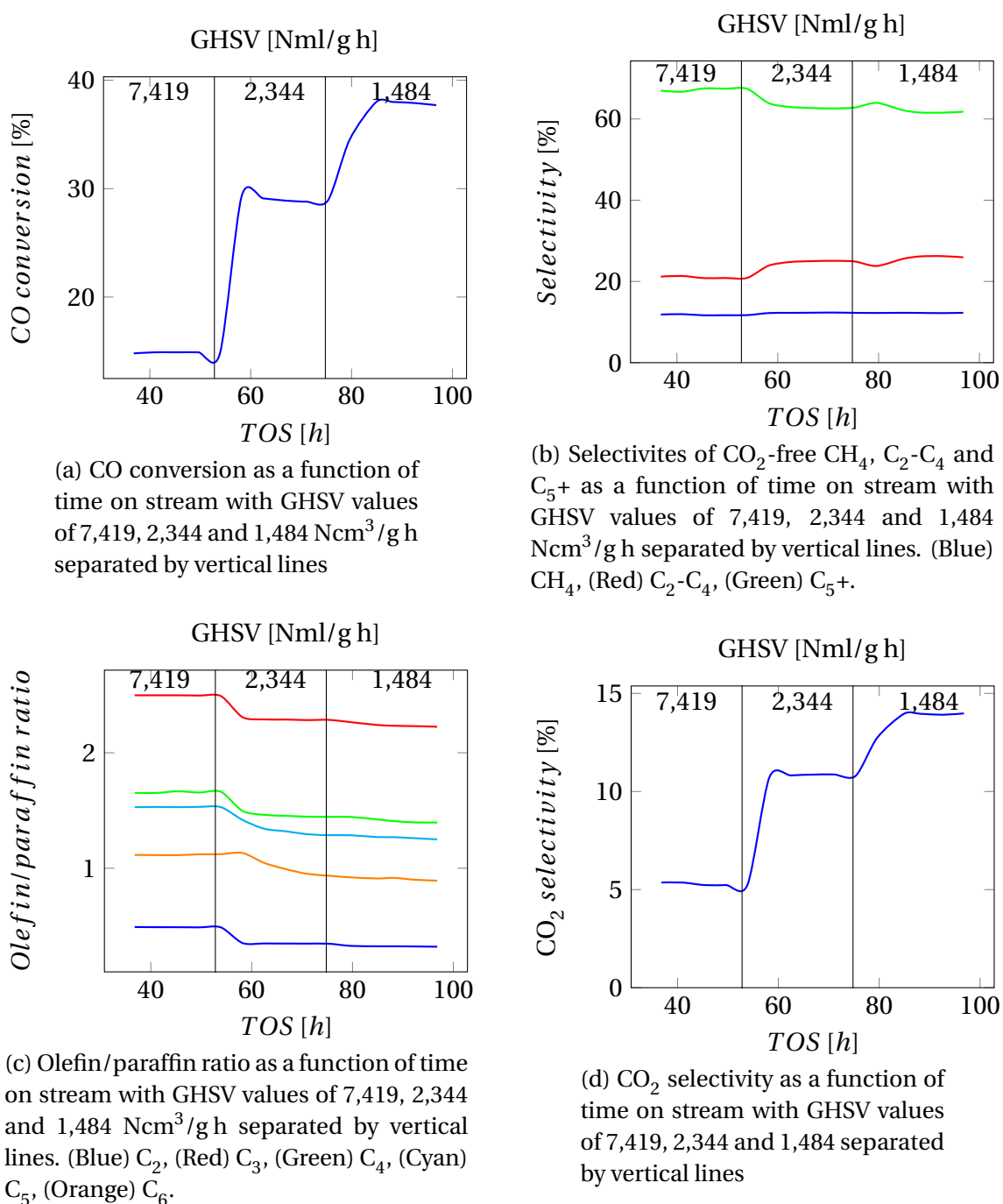


Figure 4.2: Activity and selectivity plots of the 20Fe1K catalyst at 20 bar and 230 °C reduced with hydrogen

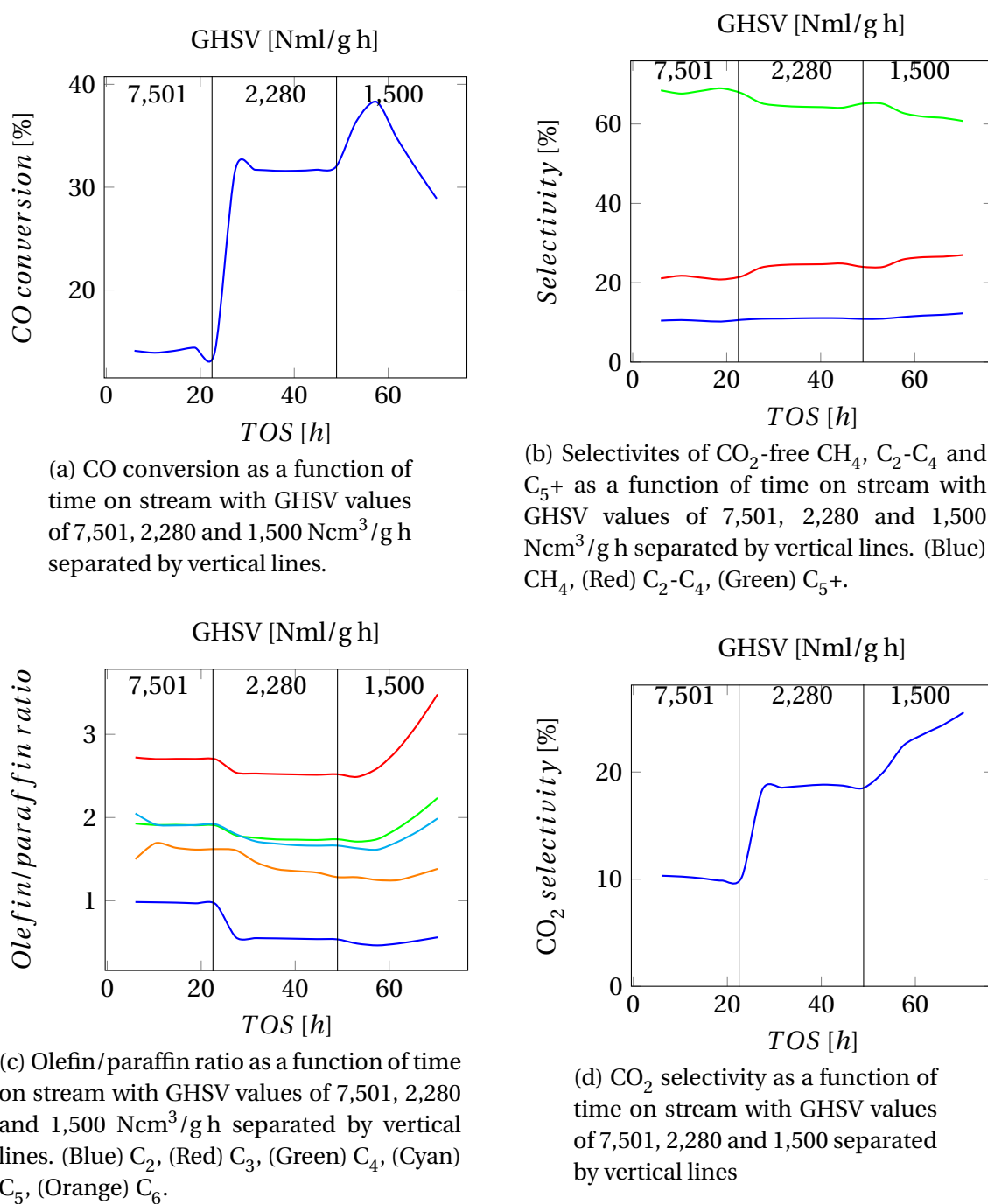


Figure 4.3: Activity and selectivity plots of the 20Fe5K catalyst at 20 bar and 230 °C reduced with hydrogen

Table 4.4: CO<sub>2</sub>-free CH<sub>4</sub>, C<sub>2</sub>-C<sub>4</sub> and C<sub>5</sub>+ selectivities for the three catalysts 20Fe, 20Fe1K and 20Fe5K at steady-state conditions and at approximately equal CO conversion levels of ~ 40%.

Catalyst	20Fe	20Fe1K	20Fe5K
ToS [h]	60.7	88.2	59.7
CO conversion [%]	38.5	38.0	41.0
CH <sub>4</sub> selectivity [%]	13.2	12.3	10.9
C <sub>2</sub> -C <sub>4</sub> selectivity [%]	28.2	26.2	24.5
C <sub>5</sub> + selectivity [%]	58.6	61.6	64.6

From Table 4.4 the presence of potassium can be seen to increase the selectivity towards long chained hydrocarbons, by reducing both the methane and C<sub>2</sub>-C<sub>4</sub> selectivities. The 20Fe5K catalyst with the highest potassium loading yielded the highest C<sub>5</sub>+ selectivity, with 20Fe1K yielding higher selectivities than 20Fe, which does not contain any potassium at all.

Table 4.5: Olefin/paraffin ratio of C<sub>2</sub>-C<sub>6</sub> hydrocarbons for the catalysts 20Fe, 20Fe1K and 20Fe5K at steady-state conditions and at approximately equal CO conversion levels.

Catalyst	20Fe	20Fe1K	20Fe5K
ToS [h]	60.7	88.2	59.7
CO conversion [%]	38.5	38.0	41.0
C <sub>2</sub> o/p ratio	0.31	0.32	0.45
C <sub>3</sub> o/p ratio	2.21	2.23	2.47
C <sub>4</sub> o/p ratio	1.38	1.41	1.68
C <sub>5</sub> o/p ratio	1.20	1.27	1.62
C <sub>6</sub> o/p ratio	0.81	0.92	1.33

Table 4.5 shows the 20Fe5K catalyst producing higher ratios of olefins versus paraffins than catalysts 20Fe and 20Fe1K, with 20Fe1K having slightly higher olefin/paraffin ratios than 20Fe.

### 4.2.3 Copper promoted catalysts

The two copper containing catalysts 20Fe2Cu5K and 30Fe2Cu5K have their activity and selectivity values depicted in Figures 4.4 and 4.5. Tables 4.6, 4.7 and 4.8 show the selectivities, activities and olefin/paraffin ratios for the two catalysts, and compare them to catalyst 20Fe5K from Section 4.2.2. 20Fe2Cu5K starts at a conversion level of about 9%, while the 30Fe2Cu5K catalyst starts at about 13.5%. The high iron content catalyst reaches higher conversion levels at steady-state, even at higher space velocities. The CO<sub>2</sub>-free selectivities are stable for all conversion levels, as shown in Figures 4.4b and 4.5b. Olefin/paraffin ratios also decrease for the two catalysts, shown in Figures 4.4c and 4.5c, with C<sub>3</sub> having the highest value. However, the olefin/paraffin ratio for catalyst 20Fe2Cu5K increases over time, and after almost 70 hours on stream are the values the same as the initial values, even though CO conversion are almost 5 times as high. Figures 4.4d and 4.5d show the selectivity of CO<sub>2</sub> to increase with increasing conversion, and for catalyst 30Fe2Cu5K the selectivity reaches values of 30% at steady-state.

Table 4.6: Activity of the catalysts 20Fe5K, 20Fe2Cu5K and 30Fe2Cu5K at 20 bar and 230 °C at initial and steady-state conditions.

Catalyst	20Fe5K		20Fe2Cu5K		30Fe2Cu5K	
	I	SS	I	SS	I	SS
ToS [h]	25.0	59.7	19.3	66.4	30.0	78.6
GHSV [Ncm <sup>3</sup> /g h]	14,139	2,262	7,517	1,503	7,330	1,759
CO conversion [%]	11.7	41.0	9.3	35.0	13.5	50.8
r <sub>CO</sub> [mol CO/g h]	0.023	0.013	0.010	0.007	0.014	0.013
STY [s <sup>-1</sup> ]	0.112	0.063	0.080	0.060	0.273	0.247

In Table 4.6 the catalyst 30Fe2Cu5K can be seen reaching CO conversions of over 50%, while the other copper containing catalyst 20Fe2Cu5K does not reach 40%, even though it had a lower value of GHSV. In comparison, the most active of the potassium-only catalysts from Section 4.2.2 - 20Fe1K and 20Fe5K - display higher rates of conversion than the 20Fe2Cu5K catalyst, but about the same values as the 30Fe2Cu5K catalyst.

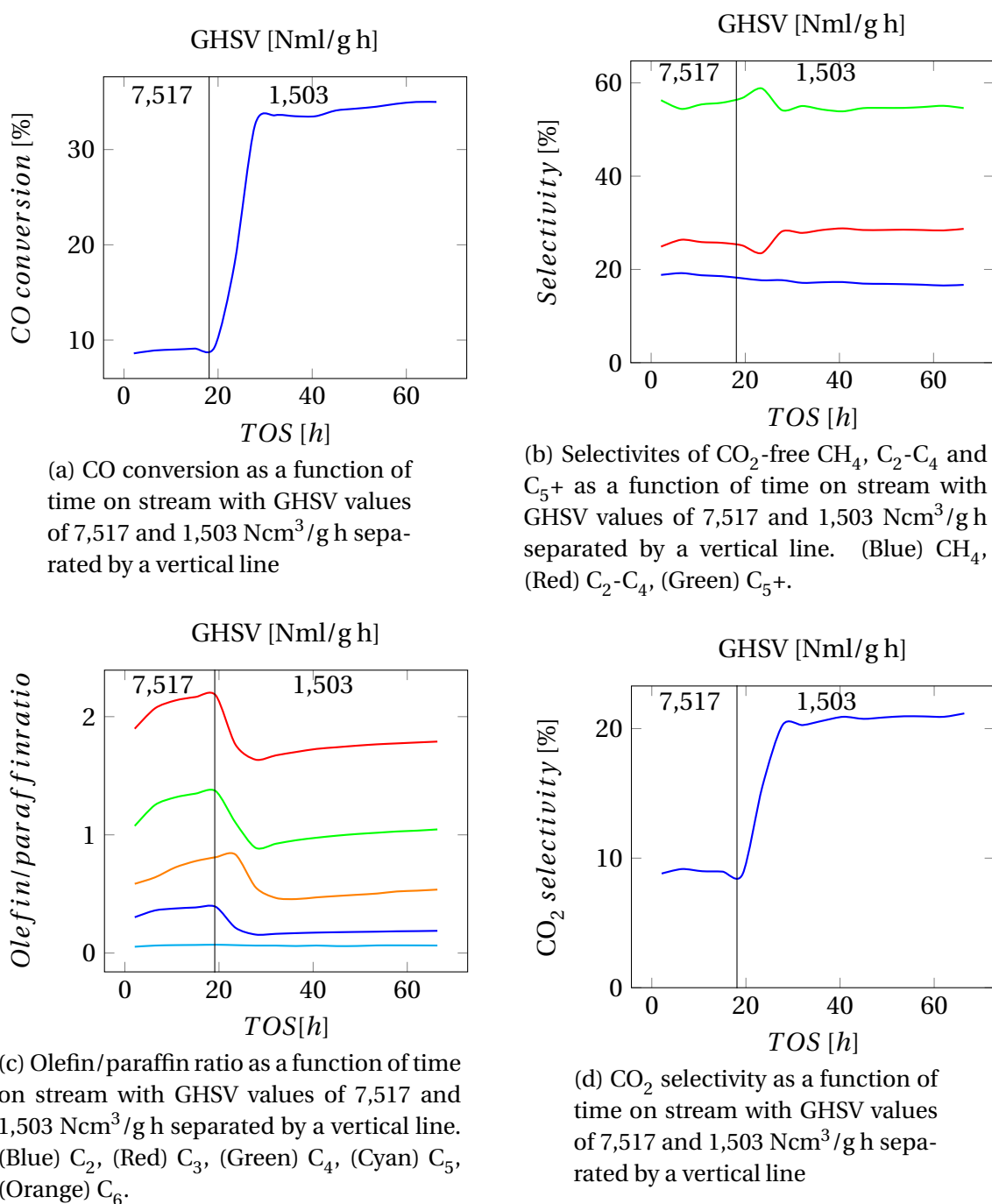


Figure 4.4: Activity and selectivity plots of the 20Fe2Cu5K catalyst at 20 bar and 230 °C reduced with hydrogen



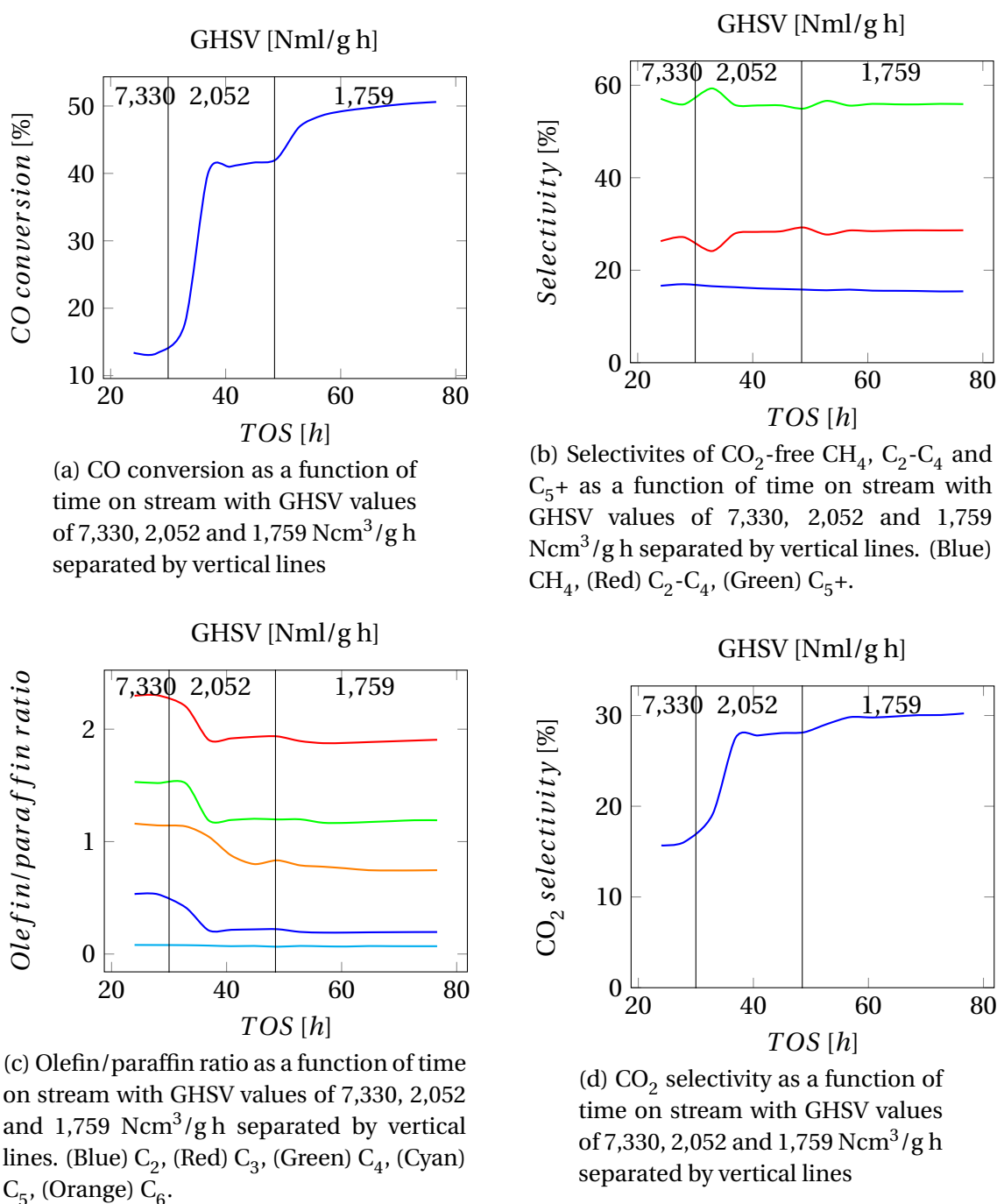


Figure 4.5: Activity and selectivity plots of the 30Fe2Cu5K catalyst at 20 bar and 230 °C reduced with hydrogen

Table 4.7: CO<sub>2</sub>-free CH<sub>4</sub>, C<sub>2</sub>-C<sub>4</sub> and C<sub>5</sub>+ selectivities for the three catalysts 20Fe5K, 20Fe2Cu5K and 30Fe2Cu5K at steady-state conditions and at approximately equal CO conversion levels of ~ 40%.

Catalyst	20Fe5K	20Fe2Cu5K	30Fe2Cu5K
ToS [h]	59.7	66.4	48.8
CO conversion [%]	41.0	35.0	42.1
CH <sub>4</sub> selectivity [%]	10.9	16.7	15.8
C <sub>2</sub> -C <sub>4</sub> selectivity [%]	24.5	28.7	29.2
C <sub>5</sub> + selectivity [%]	64.6	54.6	55.0

The selectivity towards production of long-chained hydrocarbons are higher for catalyst 20Fe5K than for 20Fe2Cu5K and 30Fe2Cu5K, as can be seen in Table 4.7. The range of selectivity values for the two copper catalysts are very similar.

Table 4.8: Olefin/paraffin ratio of C<sub>2</sub>-C<sub>6</sub> hydrocarbons for the catalysts 20Fe5K, 20Fe2Cu5K and 30Fe2Cu5K at steady-state conditions and at approximately equal CO conversion levels.

Catalyst	20Fe5K	20Fe2Cu5K	30Fe2Cu5K
ToS [h]	59.7	66.4	48.8
CO conversion [%]	41.0	35.0	42.1
C <sub>2</sub> o/p ratio	0.45	0.19	0.22
C <sub>3</sub> o/p ratio	2.47	1.79	1.94
C <sub>4</sub> o/p ratio	1.68	1.05	1.20
C <sub>5</sub> o/p ratio	1.62	0.06	0.06
C <sub>6</sub> o/p ratio	1.33	0.54	0.83

Table 4.8 shows the 20Fe5K catalyst producing higher ratios of olefins versus paraffins than catalysts 20Fe2Cu5K and 30Fe2Cu5K, with 30Fe2Cu5K having slightly higher olefin/paraffin ratios than 20Fe2Cu5K.

#### 4.2.4 Effects of syngas reduction

Figures 4.6 and 4.7 show selectivity and activity measurements for two of the experiments conducted with synthesis gas as the reduction medium. Table 4.9 lists the activity data at initial and steady-state for the two experiments, and compares them to the values obtained for the same catalysts with hydrogen as reduction medium. Table 4.10 compares the effect of synthesis gas for the CO<sub>2</sub>-free selectivities, and in Table 4.11 the effects on olefin/paraffin ratios are listed.

For the experiments conducted with synthesis gas in the activation phase, CO conversion only reaches 25% and 30% for catalysts 20Fe5K and 20Fe2Cu5K respectively, as shown in Figures 4.6a and 4.7a. Unlike the experiments using hydrogen as reduction medium, the two using synthesis gas seemed to yield higher C<sub>5</sub>+ selectivities at higher conversions, and also lower the production of methane, as shown in Figures 4.6b and 4.7b. They even produced less CO<sub>2</sub> than the corresponding hydrogen reduced catalysts, with selectivities not exceeding 12%, shown in Figures 4.6d and 4.7d. The ratios of olefins/paraffins had high initial values of around 3.5 for C<sub>3</sub>, and only slightly decreased with increasing conversion levels. The olefin/paraffin ratios are shown in Figures 4.6c and 4.7d.

Table 4.9: Activity of the catalysts 20Fe5K and 20Fe2Cu5K at 20 bar and 230 °C at initial and steady-state conditions, reduced in hydrogen and synthesis gas.

Catalyst	20Fe5K				20Fe2Cu5K			
	Hydrogen		Synthesis gas		Hydrogen		Synthesis gas	
	I	SS	I	SS	I	SS	I	SS
ToS [h]	25.0	59.7	21.4	64.3	19.3	66.4	20.3	67.5
GHSV [Ncm <sup>3</sup> /g h]	14,139	2,262	7,474	1,495	7,517	1,503	7,501	1,500
CO conversion [%]	11.7	41.0	6.5	30.4	9.3	35.0	5.4	25.1
r [mol CO/g h]	0.023	0.013	0.006	0.006	0.010	0.007	0.006	0.005
STY [s <sup>-1</sup> ]	0.112	0.063	0.033	0.031	0.080	0.060	0.046	0.043

The measurements conducted with synthesis gas as the reduction medium struggled reaching conversion rates of CO as high as the ones reduced in hydrogen. This can be seen in Table 4.9.

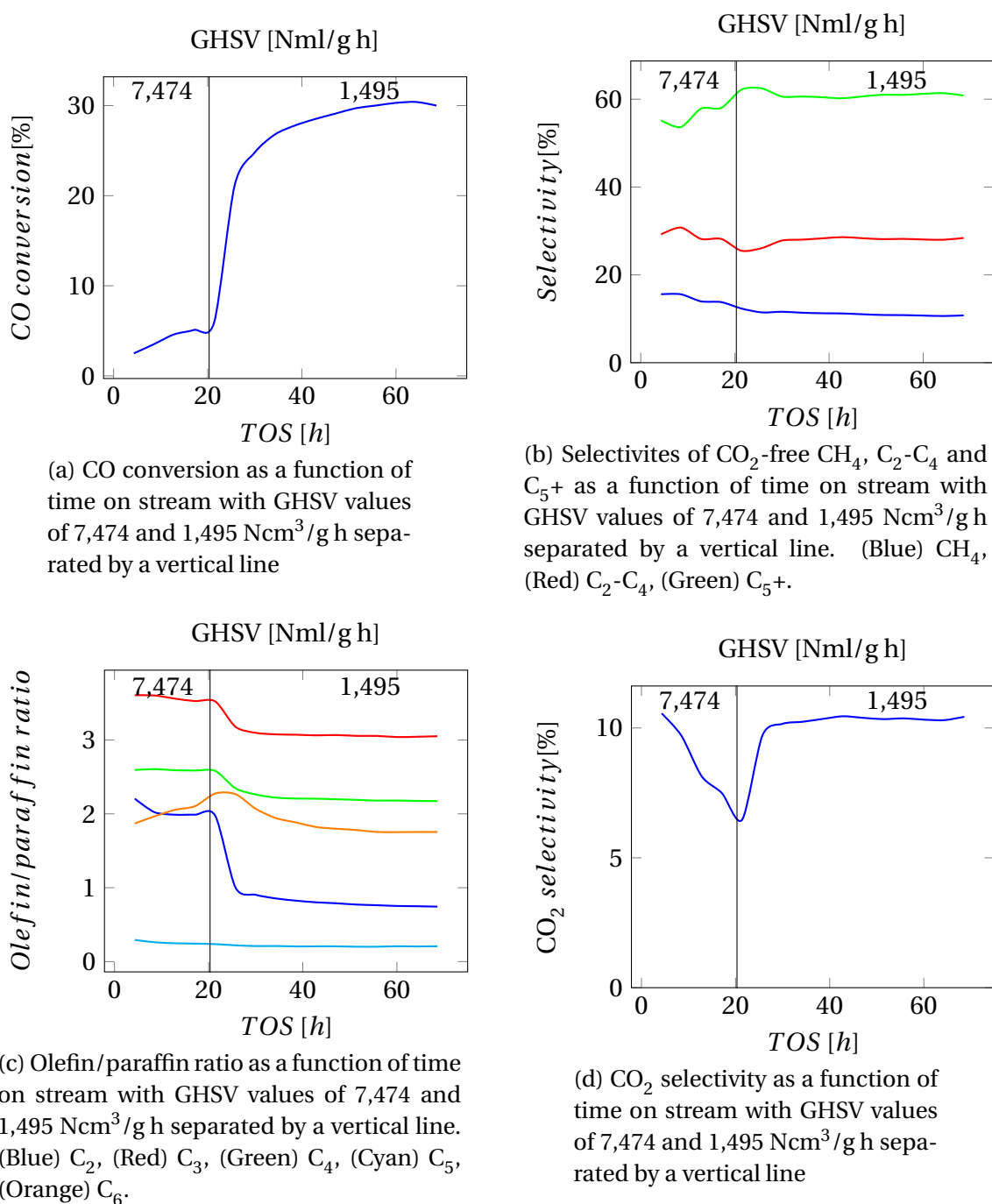


Figure 4.6: Activity and selectivity plots of the 20Fe5K catalyst at 20 bar and 230 °C reduced with syngas

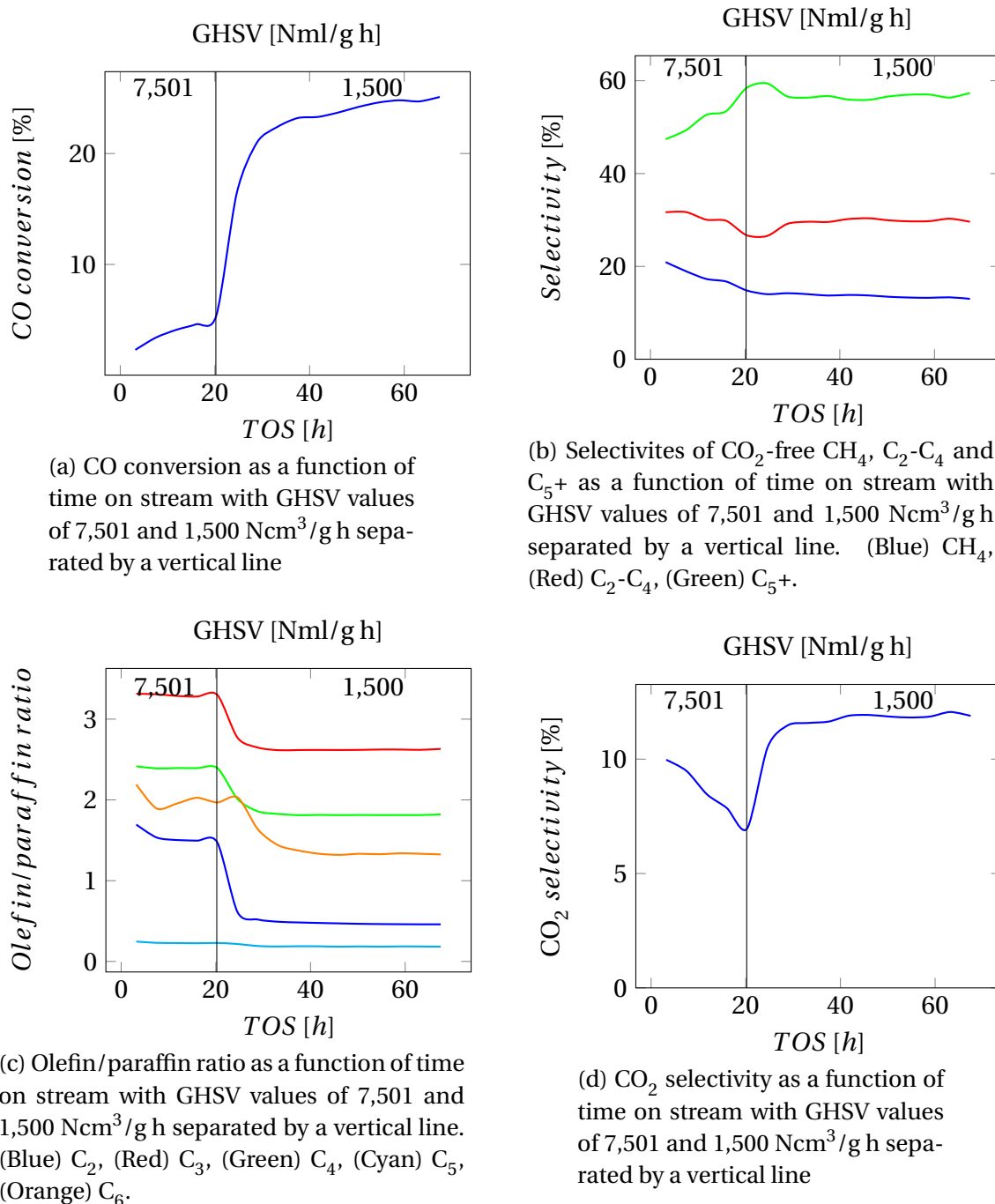


Figure 4.7: Activity and selectivity plots of the 20Fe<sub>2</sub>Cu<sub>5</sub>K catalyst at 20 bar and 230 °C reduced with syngas

Table 4.10: CO<sub>2</sub>-free CH<sub>4</sub>, C<sub>2</sub>-C<sub>4</sub> and C<sub>5</sub>+ selectivities for the two catalysts 20Fe5K and 20Fe2Cu5K at steady-state conditions and at approximately equal CO conversion levels of ~ 30%.

Catalyst	20Fe5K		20Fe2Cu5K	
	Hydrogen	Synthesis gas	Hydrogen	Synthesis gas
ToS [h]	41.9	64.3	35.9	67.5
CO conversion [%]	28.9	30.4	31.8	25.1
CH <sub>4</sub> selectivity [%]	10.5	10.6	17.5	13.0
C <sub>2</sub> -C <sub>4</sub> selectivity [%]	22.8	28.0	27.5	29.6
C <sub>5</sub> + selectivity [%]	66.7	61.4	55.0	57.4

In Table 4.10 the selectivity results are displayed at approximately the same CO conversion levels to get a better comparison between the two reduction mediums. The effect of using synthesis gas in the reduction step yields different results for the two catalysts. Catalyst 20Fe5K has a higher selectivity towards medium chained hydrocarbons when synthesis gas was used, at the expense of lower selectivity of long chained hydrocarbons. For the 20Fe2Cu5K catalyst the presence of synthesis gas gave a different result, with a slightly higher selectivity towards both medium and long chained hydrocarbons, and a significantly lower methane production. It is possible this is due to the measurements being taken at a lower conversion of CO.

Table 4.11: Olefin/paraffin ratio of C<sub>2</sub>-C<sub>6</sub> hydrocarbons for the catalysts 20Fe5K and 20Fe2Cu5K reduced in hydrogen and synthesis gas at steady-state conditions and at approximately equal CO conversion levels.

Catalyst	20Fe5K		20Fe2Cu5K	
	Hydrogen	Synthesis gas	Hydrogen	Synthesis gas
ToS [h]	41.9	64.3	35.9	67.5
CO conversion [%]	28.9	30.4	31.8	25.1
C <sub>2</sub> o/p ratio	0.59	0.75	0.16	0.46
C <sub>3</sub> o/p ratio	2.58	3.04	1.68	2.63
C <sub>4</sub> o/p ratio	1.77	2.17	0.94	1.82
C <sub>5</sub> o/p ratio	1.72	0.21	0.06	0.18
C <sub>6</sub> o/p ratio	1.44	1.75	0.82	1.33

The use of synthesis gas in the reduction step is a much more effective way of producing olefins versus paraffins as is observed from the ratios for C<sub>2</sub>-C<sub>6</sub> hydrocarbons listed in Table 4.11. All but one of the olefin/paraffin ratios increase when synthesis gas is used, even doubling some of them.

### 4.2.5 CO<sub>2</sub> selectivity

Table 4.12: CO<sub>2</sub> selectivity for the five catalysts at steady-state conditions.

<b>Catalyst</b>	<b>20Fe</b>	<b>20Fe1K</b>	<b>20Fe5K</b>		<b>20Fe2Cu5K</b>		<b>30Fe2Cu5K</b>
<b>Reduction medium</b>	<b>H<sub>2</sub></b>	<b>H<sub>2</sub></b>	<b>H<sub>2</sub></b>	<b>SG</b>	<b>H<sub>2</sub></b>	<b>SG</b>	<b>H<sub>2</sub></b>
ToS [h]	60.7	88.2	59.7	64.3	66.4	67.5	48.8
CO conversion [%]	38.5	38.0	41.0	30.4	35.0	25.1	42.1
CO <sub>2</sub> selectivity [%]	12.8	14.0	21.8	10.3	21.2	11.9	28.2

Table 4.12 lists the selectivity of CO<sub>2</sub> production for all the catalysts and the different reduction mediums, hydrogen and synthesis gas. The values are taken at CO conversion levels of approximately 40%, except for the two catalysts reduced in synthesis gas, which were not able to reach conversion levels high enough. The highest production of CO<sub>2</sub> was reached using the catalyst 30Fe2Cu5K containing the largest percentage of iron, but also the catalysts 20Fe5K and 20Fe2Cu5K had selectivities over 20%.





# Chapter 5

## Discussion

The discussion section addresses three main areas of interest, the preparation of the catalysts, characterization, and the activity and selectivity measurements.

### 5.1 Catalyst preparation

#### 5.1.1 Choice of catalyst promoters

As discussed in Section 2.2.1, the choice of materials for preparing the catalyst was based on results from previously published articles. Alumina was preferred as the support material despite many reports suggesting it to have lower surface areas and pore volumes than silica supports. Alumina was still chosen due to previous reports claiming it to have higher values of CO conversion, it being easily accessible, and due to its lower selectivity towards methane, which is an undesired product for the FTS. The CO conversion for alumina support was reported as higher than for silica, both initially and at steady-state, but it needed a longer period of time on stream in order to reach its maximum conversion<sup>[4]</sup>.

For the promoters, several transition metals and alkali metals were considered by looking at the effects they have on conversion rates and their selectivity towards long chained hydrocarbons and methane. The most interesting materials were presented in Section 2.2.1, but due to the limited time frame only a few materials were chosen for fabrication, focusing instead on different loading values. The effects of potassium were very interesting, having positive effects on both conversion and methane selectivity. The conversion levels also increased for copper, which is another often used promoter for iron FT catalysts, and the effects seemed to be even stronger when both materials were used together. Copper did not show the same trends for selectivity, as it would increase the methane selectivity in the

reaction. This could however be fixed by adding potassium to the catalyst, as catalysts containing both promoter materials had lower methane selectivity than catalysts without promoters.

Effects of zinc and silicon oxide were also presented, but only two promoters were chosen for catalyst preparation. Potassium and copper seemed to be a necessity for all good iron catalysts. However, potassium may also improve a catalyst on its own, and enhance the formation of long chain and olefinic hydrocarbons<sup>[17]</sup>. It was decided to make catalysts with both potassium and copper, as well as some with only potassium. Even though potassium showed positive results, the effects seemed to wear off at atomic ratios higher than 5/100 to iron, thus it was decided to not make catalysts with higher ratios<sup>[16]</sup>.

Three catalysts were made in order to study the potassium effects on the product distribution. One catalyst, 20Fe, was prepared without any potassium, and the two others, 20Fe1K and 20Fe5K, were prepared with K/Fe ratios of 1/100 and 5/100 respectively.

Two copper catalysts were prepared, one with 20 wt% iron as the three first catalysts, and one with an iron loading of 30 wt%, in hope of having higher activity, or higher selectivity towards desired products. The copper to iron ratio was fixed to 2/100 for the two catalysts, and the potassium to iron ratio was the same 5/100 as for the 20Fe5K catalyst.

### **5.1.2 Incipient wetness method**

On the basis of literature surveys it was decided the catalysts should contain 20 weight percent of iron, with one catalyst containing 30 wt% for comparison. Due to restrictions in the solubility of iron nitrate, it was not possible to reach the required loadings in only one step. The iron therefore had to be added in two and three impregnation steps, with drying and calcination after each step. A support material with larger pores and higher surface area could possibly have the iron impregnated in only one step. When the incipient wetness point was found, it was calculated from the same sample that was eventually going to be made into a finished catalyst. In this way no extrapolations were needed, which could later have led to the wrong amount of water being weighed. The catalyst was calcined at 300 °C for 16 hours after each impregnation step, a procedure reported in several articles. By calcining the catalyst precursor between the impregnation steps, the metal particles were transformed into oxides on the alumina surface. A higher dispersion could possibly have been obtained if all the metal had been impregnated before calcination occurred. Copper nitrate did not experience the same limitations in solubility, but since it was co-impregnated with iron it also had to be loaded in multiple steps. Potassium was not added to the catalyst

with co-impregnation, but instead in a separate step after the iron and copper were added.

## 5.2 Catalyst characterization

The results from the catalyst characterizations are discussed in this section, with the chemisorption discussion in Section 5.2.1 and the physisorption in Section 5.2.2.

### 5.2.1 Chemisorption

The dispersion of iron on the surface was calculated to have a wide range of values from 0.27 to 1.65%. These are low values and could indicate the iron not loading itself onto the alumina surface in monolayers, but rather in multiple layers, which could lead to a lower activity. However, iron generally has low dispersion values<sup>[8]</sup>, so this is not unprecedented. The catalyst 30Fe2Cu5K was found to have the lowest dispersion, even though it had the largest amount of iron of all the catalysts. This is most likely an effect of inaccuracies in the preparation of the catalyst. The catalyst precursors were chosen to be dried and calcined after each impregnation step. This may indicate the iron loaded in the second and third impregnation step was loaded onto the iron already present on the catalyst surface, thus yielding several metal layers. This could be especially true for the catalyst 30Fe2Cu5K, which required the largest number of impregnation steps, and also had the lowest value of dispersion.

### 5.2.2 Physisorption

Section 4.1.2 in Chapter 4 presents the results for surface area and pore size distribution. As predicted the surface area of alumina decreases as iron is loaded onto it, from an initial value of 161.4 m<sup>2</sup>/g to 128.5 m<sup>2</sup>/g, and even further to 108.0 m<sup>2</sup>/g for the catalyst with 30 wt% iron loading. This last value is not fully comparable, as the catalyst 30Fe2Cu5K also contains two types of promoters which could affect the surface area. Studying the surface area values for the other promoter containing catalysts, it may be observed that the inclusion of promoters does not have a significant effect. For instance, the inclusion of copper has almost no effect on surface area, as the values for catalysts 20Fe5K and 20Fe2Cu5K are almost the same.

A similar trend is observed for the pore volumes of the samples, most apparent with the 20Fe5K catalyst, which decreases from 0.68 cm<sup>3</sup>/g from the alumina to 0.43 cm<sup>3</sup>/g for the finished product.

## 5.3 Activity and selectivity measurements

This section covers the measurement discussion of the experiments conducted in the Fischer-Tropsch rig. Section 5.3.1, 5.3.2, and 5.3.3 discuss the activity, selectivity and olefin/paraffin ratios respectively. The effects of the use of syngas in the activation step on these aforementioned parameters are discussed in Section 5.3.4.

### 5.3.1 Activity

Initially the objective was to compare selectivity and olefin/paraffin ratios at CO conversion levels of 50%, due to this being the standard for previous catalyst testing in the rig. However, the iron catalysts had difficulties reaching conversion levels of 50% without running at unreasonably low space velocities. The rig is ordinarily run using cobalt based catalysts, and the catalysts prepared in this project were in fact the first iron based catalysts to be tested in the rig<sup>[28]</sup>. Though iron catalysts are less expensive, are they not as active as cobalt catalysts, which caused the troubles reaching satisfactory conversion levels. The experiments instead aimed for conversion levels of 35-40%.

One catalyst stood out among all the others regarding activity. The catalyst 30Fe2Cu5K managed to reach a conversion level of CO of just over 50%, while running at the same space velocities as the other catalysts. This high activity may also be seen in the values of the site time yield. This is defined as the rate of CO hydrogenated per surface iron atom per second and was calculated using Equation 2.8 in Section 2.5. STY values are a good indication of activity, as it take into account not only the rate of CO reacted, but also accommodates for the dispersion of metal. On the basis of dispersion values in Table 4.1 and the reaction rates, the STY values are presented in Tables 4.3 and 4.6. It is impressive for the catalyst to reach the high level of conversion and still have the lowest dispersion of all the catalysts. This is most likely due to the higher amount of iron, giving reason to believe iron is the single most essential metal regarding catalyst activity. 30Fe2Cu5K had an iron loading of 30 wt%, 50% higher than all other catalysts, and twice as high STY value at steady-state as the next catalyst, 20Fe1K. Though initial STY values for the two catalysts were about equal, the 20Fe1K catalyst halved its STY value at steady-state. This was also observed for the other catalysts, except when syngas was used in the activation step, which will be discussed in Section 5.3.4.

### 5.3.2 Selectivity

Selectivity is defined as the number of moles of a specific product produced per moles of total products. On the basis of Tables 4.4 and 4.7 in Section 4.2 the effect of potassium is clearly observed. The selectivity towards long chained hydrocarbons,  $C_5$  and higher, increases with potassium content, which at the same time directly causes the methane and  $C_2$ - $C_4$  selectivities to decrease.

The same effects are not observed for the copper containing catalysts. On the contrary, the addition of copper causes the selectivity of  $C_5+$  hydrocarbons to decrease, with the production of methane increasing about 50% for catalyst 20Fe2Cu5K compared to 20Fe5K. This is in accordance with the findings from literature reported in Section 2.2.1. It was expected for the potassium to have a positive effect on production of long chained hydrocarbons, while copper would more likely promote the production of methane. However, for catalysts containing both metals, the two opposing effects were expected to cancel each other out. This was not the case for catalyst 20Fe2Cu5K, as it had both higher selectivity value for methane and lower  $C_5+$  values than catalyst 20Fe, which was prepared without any promoters.

### 5.3.3 Olefin/paraffin ratios

Olefin versus paraffin production was measured for hydrocarbons of five different lengths,  $C_2$  to  $C_6$ . Independent of catalyst, the o/p-ratio was always highest for hydrocarbons of  $C_3$ , and lowest for  $C_2$  hydrocarbons. Tables 4.5 and 4.8 in Section 4.2 shows the o/p-ratios at steady-state for all five catalysts. From these it is evident the inclusion of potassium promotes an increase in ratio. More potassium leads to higher production of olefins compared to paraffins.

The introduction of copper was found to have the opposite effect of potassium. The copper containing catalysts 20Fe2Cu5K and 30Fe2Cu5K yields much lower o/p-ratios than any of the other catalysts, even the plain 20Fe catalyst. The literature is not clear on the effects of potassium and copper on iron catalysts regarding the o/p-ratio. Most sources report only small variations in the ratios, and none of them show results that differs as much as the ones measured in this thesis.

The slight difference between results obtained with catalysts 20Fe2Cu5K and 30Fe2Cu5K must also be noted. The higher amount of iron present seems to yield a higher ratio for the olefin production, and it could be interesting to observe if an high iron content catalyst without copper would produce even higher o/p-ratios.

### 5.3.4 Hydrogen and syngas activation

Two of the catalysts, 20Fe5K and 20Fe2Cu5K, were run in the Fischer-Tropsch rig exposed to syngas during the activation step. The results are reported in Section 4.2.4. None of the two experiments reported in the results managed to reach CO conversion levels even close to 40% at low space velocities. The 20Fe5K catalyst reached the highest conversion of 30.4% at steady-state, as listed in Table 4.9. Even the STY values were lower than for any of the experiments conducted with hydrogen. It is worth noticing the STY values did not decline from initial to steady-state, but considering their very low initial values, there were hardly any room for changes.

Due to a misunderstanding in at the laboratory, the stream of syngas was found to have been cut off for a couple of minutes during cooling after activation. The low activity could be explained by deactivation of the catalysts during the short uphold of stream through the reactor. It was therefore decided to replicate the experiments one more time. The results from these runs are depicted in Figure D.3 and D.4 in Appendix D. Strangely enough these new experiments showed even less activity than the original ones, ultimately leading to an abortion after about 48 hours on stream.

The syngas activation had different effects on the selectivity results from the two hydrogen activated catalysts. For catalyst 20Fe5K the syngas activation had a negative effect regarding the selectivity towards long chained hydrocarbons, producing five percentage points less  $C_5+$  at steady-state. This did not affect the methane production, as the selectivity towards methane had the same values for the two experiments. Catalyst 20Fe2Cu5K produced slightly more  $C_5+$  and medium length hydrocarbons after it was exposed to syngas, and considerably less methane. The discrepancy between results obtained with different activation methods could be explained by the large difference in the conversion levels the two numbers were compared at. The experiment using syngas settled at conversion levels of about 25%, while the experiment using hydrogen never stabilized around those values. The closest value for hydrogen activated catalyst came at CO conversions of 35%, a much higher level than the one obtained for the syngas activated one. From Figure 4.4b and 4.7b it can be seen that the selectivity towards long chained hydrocarbons decreases at higher conversion levels for the catalyst activated in hydrogen, while the same selectivity increases with higher conversion for the other catalyst. This may indicate that the syngas activated catalyst could yield higher  $C_5+$  selectivity at comparable CO conversion levels.

Table 4.11 indicates that the presence of syngas yields higher ratios of olefin compared to paraffins for both catalysts. Catalyst 20Fe5K has a propene to propane ratio of 3.04 at steady-

state, the highest o/p-ratio value for any catalyst at any hydrocarbon length. Once again, the conversion levels of the two experiments with 20Fe5K catalyst are comparable, but for the catalyst 20Fe2Cu5K the levels are too far apart to conclude anything, especially considering Figure 4.7c where the o/p-ratio decreases with increasing CO conversion. However, as most ratio values are much higher for the catalyst activated in syngas, with some reaching double values, the effect of syngas activation may still be relevant.

### 5.3.5 CO<sub>2</sub> production

The production of CO<sub>2</sub> is an unwanted side reaction in the Fischer-Tropsch synthesis. This is known as the Boudouard reaction, mentioned in Section 2.1.2, and Table 4.12 lists the amount of CO<sub>2</sub> produced for the five catalysts. There are three experiments which clearly distinguish themselves from the others. The catalysts 20Fe5K and 20Fe2Cu5K activated in hydrogen have selectivities of 21-22%, while the catalyst 30Fe2Cu5K produces CO<sub>2</sub> with a selectivity of over 28%. These are very high values, and are not compatible with use in the industry, which require much lower values<sup>[12]</sup>. The four other experiments have selectivities from 10% to 14%, with the catalysts activated by the syngas yielding the lowest values. There is reason to believe the high CO<sub>2</sub> selectivity for catalyst 30Fe2Cu5K is due to its high content of iron, but it seems the high iron content only enhances an effect already existing. An experiment conducted with a high loading iron catalyst consisting of less potassium and copper could indicate which factor has the highest effect, promoters or iron. In general, the catalysts with the highest promoter material content produced the largest amount of CO<sub>2</sub>.





# Chapter 6

## Conclusions

### 6.1 Summary and conclusions

The objective of this work was to study the effects of promoter materials on an iron catalyst. The effects studied were activity, selectivity, as well as production of olefins versus paraffins. Five catalysts were fabricated, all with different loadings of potassium and copper. All catalysts were prepared using the same preparation method, incipient wetness method, followed by drying and calcination. In addition to testing them in a Fischer-Tropsch rig, they were also characterized using chemisorption and physisorption techniques.

The iron was loaded onto the support using aqueous solutions of iron nitrate, but due to low solubility, iron had to be loaded in multiple steps. This may have led to low and uneven distribution of the iron on the catalyst support, resulting in a lower activity. This was observed for the catalyst 30Fe2Cu5K, which required the largest amount of impregnation steps, and also showed to have the lowest dispersion value.

Potassium proved to have the greatest effect on selectivity towards desired products, namely long chained hydrocarbons and olefins. This was expected, as the literature survey had produced several sources reporting the same findings. The use of copper as a promoter was expected to yield higher conversions of CO, at the cost of higher selectivity of methane. The results were rather disappointing, as the activity and conversion levels both decreased, as did the selectivity towards desired products. One of the copper containing catalysts, 30Fe2Cu5K, did show high activity values, but this was probably due to a higher iron content.

Replacing hydrogen with syngas in the activation step also made the catalysts less active, and selectivity towards the long chained hydrocarbons decreased. The syngas activated cat-

alysts did however produce much larger quantities of olefins versus paraffins than the other experiments.

The production of  $\text{CO}_2$ , which is an unwanted side reaction in the Fischer-Tropsch synthesis was clearly highest for the 30Fe2Cu5K catalyst. Generally the catalysts with the highest promoter material content produced the largest amount of  $\text{CO}_2$ , except the ones activated by syngas.

## 6.2 Recommendations for further work

Catalyst 30Fe2Cu5K showed more promising results with high activity and higher olefin selectivities than its accompanying catalyst 20Fe2Cu5K, but also displayed some negative results, chiefly its very high  $\text{CO}_2$  production. It would be interesting to make a catalyst with as high or possibly even higher iron content, without copper, which seemed to limit the potential of the catalyst.

Other preparation methods for the catalysts could be looked into. Using the incipient wetness method required the iron to be loaded on the support in multiple steps. This may have lead to lower dispersions. By using other techniques, where the metal is loaded on to the support in one step, the activity could possibly be increased.

The catalysts could also have been tested in the micro-channeled reactor.

# Bibliography

- [1] *U.S. Energy Information Administration.*
- [2] *U.S. Energy Information Administration.*
- [3] *U.S. Energy Information Administration.*
- [4] R. J. O'Brien, L. Xu, S. Bao, A. Raje, and B. H. Davis, "Activity, selectivity and attrition characteristics of supported iron fischer-tropsch catalysts," *Applied Catalysis A: General*, vol. 196, no. 2, pp. 173 – 178, 2000.
- [5] E. Iglesia, S. Li, A. Li, and S. Krishnamoorthy, "Effects of zn, cu, and k promoters on the structure and on the reduction, carburization, and catalytic behavior of iron-based fischer-tropsch synthesis catalyst," vol. 77, no. 4, 2001.
- [6] H. Hayakawa, H. Tanaka, and K. Fujimoto, "Studies on precipitated iron catalysts for fischer-tropsch synthesis," *Applied Catalysis A: General*, vol. 310, no. 0, pp. 24 – 30, 2006.
- [7] H. Schulz, "Short history and present trends of fischer-tropsch synthesis," *Applied Catalysis A: General*, vol. 186, no. 1–2, pp. 3 – 12, 1999.
- [8] D. Schanke, *Hydrogenation of CO over supported iron catalysts*. The laboratory of Industrial Chemistry, The University of Trondheim, The Norwegian Institute of Technology, 1986.
- [9] C. Pirola, "Fischer tropsch and water gas shift chemical regimes on supported iron-based catalysts at high metal loading," *Catalysis Communications*, vol. 10, 2008.
- [10] A. Steynberg, M. Dry, B. Davis, and B. Breman, "Chapter 2 - fischer-tropsch reactors," in *Fischer-Tropsch Technology* (A. Steynberg and M. Dry, eds.), vol. 152 of *Studies in Surface Science and Catalysis*, pp. 64 – 195, Elsevier, 2004.

## BIBLIOGRAPHY

---

- [11] P. C. Painter and M. M. Coleman, *Fundamentals of Polymer Science*. CRC Press, 2. ed., 1997.
- [12] J. Moulijn, M. Makkee, and A. E. van Diepen, *Chemical Process Technology*. John Wiley & Sons Ltd, 2. ed., 2013.
- [13] T. Riedel, M. Claeys, H. Schulz, G. Schaub, S.-S. Nam, K.-W. Jun, M.-J. Choi, G. Kishan, and K.-W. Lee, "Comparative study of fischer-tropsch synthesis with  $\text{H}_2/\text{CO}$  and  $\text{H}_2/\text{CO}_2$  syngas using Fe- and Co-based catalysts," *Applied Catalysis A: General*, vol. 186, no. 1–2, pp. 201 – 213, 1999.
- [14] H. Pichler, "Twenty-five years of synthesis of gasoline by catalytic conversion of carbon monoxide and hydrogen," vol. 4 of *Advances in Catalysis*, pp. 271 – 341, Academic Press, 1952.
- [15] D. B. Bukur and C. Sivaraj, "Supported iron catalysts for slurry phase fischer-tropsch synthesis," *Applied Catalysis A: General*, vol. 231, no. 1–2, pp. 201 – 214, 2002.
- [16] M. Luo, R. J. O'Brien, S. Bao, and B. H. Davis, "Fischer-tropsch synthesis: induction and steady-state activity of high-alpha potassium promoted iron catalysts," *Applied Catalysis A: General*, vol. 239, no. 1–2, pp. 111 – 120, 2003.
- [17] D. Bukur, "Binder/support effects on the activity and selectivity of iron catalysts in the fischer-tropsch synthesis," 1990.
- [18] K. Keyvanloo, "Effects of preparation variables on an alumina-supported Fe-Cu fischer-tropsch catalyst," *Catalysis, Science and Technology*, 2014.
- [19] I. Chorkendorff and J. Niemantsverdriet, *Concepts of Modern Catalysis and Kinetics*. John Wiley & Sons Ltd, 2006.
- [20] K. P. de Jong, *Synthesis of Solid Catalysts*. John Wiley & Sons Ltd, 2009.
- [21] J. R. Regalbuto, *Catalyst Preparation: Science and Engineering*. CRC Press, 2007.
- [22] K. Keyvanloo, M. K. Mardkhe, T. M. Alam, C. H. Bartholomew, B. F. Woodfield, and W. C. Hecker, "Supported iron fischer-tropsch catalyst: Superior activity and stability using a thermally stable silica-doped alumina support," *ACS Catalysis*, vol. 4, 2014.

- 
- [23] M. L. Cubeiro, H. Morales, M. R. Goldwasser, M. Pérez-Zurita, F. González-Jiménez, and C. U. de N, "Hydrogenation of carbon oxides over Fe/Al<sub>2</sub>O<sub>3</sub> catalysts," *Applied Catalysis A: General*, vol. 189, no. 1, pp. 87 – 97, 1999.
- [24] K. Pansanga, N. Lohitharn, A. C. Chien, E. Lotero, J. Panpranot, P. Praserthdam, and J. G. G. Jr., "Copper-modified alumina as a support for iron Fischer-Tropsch synthesis catalysts," *Applied Catalysis A: General*, vol. 332, no. 1, pp. 130 – 137, 2007.
- [25] S.-H. Kang, J. W. Bae, K.-J. Woo, P. S. Prasad, and K.-W. Jun, "ZSM-5 supported iron catalysts for Fischer-Tropsch production of light olefin," *Fuel Processing Technology*, vol. 91, no. 4, pp. 399 – 403, 2010. 7th China-Korea Workshop on Clean Energy Technology.
- [26] O. Tronstad, *Overflate- og porefordelingsmålinger*. Institutt for industriell kjemi, NTH, 1992.
- [27] R. Myrstad, *FT-rigg: Apparatur og prosedyrer for 4-reaktors fixed bed rigg*. SINTEF.
- [28] R. Myrstad. Personal communication.
- [29] M. Boudart, "Turnover rates in heterogeneous catalysis," *Chemical reviews*, vol. 95, 1995.



# **Appendix A**



## **Risk assessment**

The risk assessment of the experiments and the laboratory work is included in this appendix.

The basis for the evaluations has been the NTNU HSE Handbook and the safety datasheets for the instruments. Existing safety measures are listed in the forms.

Also included in the evaluation are the likelihoods and consequences for different activities, based on the risk matrix at the end of the assessment.

# APPENDIX A. RISK ASSESSMENT

NTNU	Hazardous activity identification process	Prepared by	Number	Date	
		HSE section	HMSRV2601E	09.01.2013	
HSE		Approved by		Replaces	
		The Rector		01.12.2006	

**Unit:** (Department)

**Date:** 16.01.2015

**Line manager:**

**Participants in the identification process** (including their function):

**Short description of the main activity/main process:** Master project for student xx. Project title.

**Is the project work purely theoretical?** (YES/NO):



Answer "YES" implies that supervisor is assured that no activities requiring risk assessment are involved in the work. If YES, briefly describe the activities below. The risk assessment form need not be filled out.

**Signatures:** Responsible supervisor:

Student:

ID nr.	Activity/process	Responsible person	Existing documentation	Existing safety measures	Laws, regulations etc.	Comment
1	Catalyst characterization: <b>Chemisorption</b>	Nils-Olav Hole	NTNU HSE Handbook	Safety goggles, gloves, lab coat, leak test, detection system	Safety datasheet, lab training	Flammable and combustible gases (CO, H <sub>2</sub> ), heat treatment
2	Catalyst characterization: <b>BET</b>	Nils-Olav Hole	NTNU HSE Handbook	Safety goggles, gloves, lab coat	Safety datasheet, lab training	Liquid nitrogen
3	Catalyst preparation: <b>Calsination</b>	Nils-Olav Hole	NTNU HSE Handbook	Safety goggles, gloves, detection system, ventilation	Safety datasheet, lab training	High temperature (300 °C)
	Catalyst testing: <b>Fischer-Tropsch rig</b>					
4	Loading of reactor	Nils-Olav Hole, Rune Myrstad		Safety goggles, gloves, lab coat	Safety datasheet, lab training	
5	Installment of reactor	Nils-Olav Hole, Rune Myrstad	NTNU HSE Handbook	Safety goggles, gas alarm, ventilation, emergency stop	Safety datasheet, FTS setup manual	



NTNU	<b>Hazardous activity identification process</b>	Prepared by	Number	Date	
		HSE section	HMSRV2601E	09.01.2013	
HSE		Approved by		Replaces	
		The Rector		01.12.2006	

<b>6</b>	Leak testing	Nils-Olav Hole, Rune Myrstad	NTNU HSE Handbook	Safety goggles, gas alarm, ventilation, emergency stop	Safety datasheet, FTS setup manual, lab training	High pressure (20 bar)
<b>7</b>	Reaction experiment	Nils-Olav Hole, Rune Myrstad	NTNU HSE Handbook	Safety goggles, gas alarm, ventilation, emergency stop	Safety datasheet, lab training	High pressure (20 bar), high temperature (230 °C)
<b>8</b>	Product removal	Nils-Olav Hole, Rune Myrstad	NTNU HSE Handbook	Visor, heat-resistant gloves	Safety datasheet, lab training	Hot wax spill

# APPENDIX A. RISK ASSESSMENT

NTNU	Risk assessment	Prepared by	Number	Date	
		HSE section	HMSRV2603E	04.02.2011	
HSE/KS		Approved by		Replaces	
		The Rector		01.12.2006	

**Unit:** *(Department)*

**Date:**

**Line manager:**


**Participants in the identification process** (including their function):

**Short description of the main activity/main process:** Master project for student xx. Project title.

**Signatures:** *Responsible supervisor:*

*Student:*

Activity from the identification process form	Potential undesirable incident/strain	Likelihood:	Consequence:			Risk Value (human)	Comments/status Suggested measures
		Likelihood (1-5)	Human (A-E)	Environment (A-E)	Economy/material (A-E)		
Catalyst characterization: <b>Chemisorption</b>	Poisoning, fire, explosion, chemical exposure, skin burn	1	E	A	A	<b>E1</b>	Compulsory instrument training
Catalyst characterization: <b>Chemisorption</b>	Leakage of gas	4	B	A	A	<b>B4</b>	Compulsory instrument training
Catalyst characterization: <b>BET</b>	Chemical exposure, skin burn	2	A	A	A	<b>A2</b>	Compulsory instrument training
Catalyst characterization: <b>BET</b>	Liquid nitrogen spill	4	B	A	A	<b>B4</b>	Compulsory instrument training
Catalyst preparation: <b>Calsination</b>	Chemical exposure, skin burn	3	B	A	A	<b>B3</b>	Compulsory instrument training
<b>Fischer-Tropsch rig</b>							

NTNU	Risk assessment	Prepared by	Number	Date	
		HSE section	HMSRV2603E	04.02.2011	
HSE/KS		Approved by		Replaces	
	The Rector		01.12.2006		

Activity from the identification process form	Potential undesirable incident/strain	Likelihood:	Consequence:			Risk Value (human)	Comments/status Suggested measures
Loading of reactor	Chemical exposure	4	A	A	A	<b>A4</b>	
Installment of reactor	Gas leakage	2	A	A	A	<b>A2</b>	
Leak testing	Gas leakage	2	A	A	A	<b>A2</b>	
Reaction experiment	Chemical exposure	4	A	A	A	<b>A2</b>	
Product removal	Chemical exposure, skin burn	3	B	A	A	<b>B3</b>	

**Likelihood, e.g.:**

1. Minimal
2. Low
3. Medium
4. High
5. Very high

**Consequence, e.g.:**

- A. Safe
- B. Relatively safe
- C. Dangerous
- D. Critical
- E. Very critical

**Risk value (each one to be estimated separately):**

- Human = Likelihood x Human Consequence**  
**Environmental = Likelihood x Environmental consequence**  
**Financial/material = Likelihood x Consequence for Economy/materiel**

**Potential undesirable incident/strain**

Identify possible incidents and conditions that may lead to situations that pose a hazard to people, the environment and any materiel/equipment involved.

**Criteria for the assessment of likelihood and consequence in relation to fieldwork**

Each activity is assessed according to a worst-case scenario. Likelihood and consequence are to be assessed separately for each potential undesirable incident. Before starting on the quantification, the participants should agree what they understand by the assessment criteria:

**Likelihood**

APPENDIX A. RISK ASSESSMENT

NTNU	Risk assessment	Prepared by	Number	Date	
		HSE section	HMSRV2603E	04.02.2011	
HSE/KS		Approved by		Replaces	
	The Rector		01.12.2006		

Minimal 1	Low 2	Medium 3	High 4	Very high 5
Once every 50 years or less	Once every 10 years or less	Once a year or less	Once a month or less	Once a week

**Consequence**

Grading	Human	Environment	Financial/material
<b>E</b> Very critical	May produce fatality/ies	Very prolonged, non-reversible damage	Shutdown of work >1 year.
<b>D</b> Critical	Permanent injury, may produce serious serious health damage/sickness	Prolonged damage. Long recovery time.	Shutdown of work 0.5-1 year.
<b>C</b> Dangerous	Serious personal injury	Minor damage. Long recovery time	Shutdown of work < 1 month
<b>B</b> Relatively safe	Injury that requires medical treatment	Minor damage. Short recovery time	Shutdown of work < 1week
<b>A</b> Safe	Injury that requires first aid	Insignificant damage. Short recovery time	Shutdown of work < 1day

The unit makes its own decision as to whether opting to fill in or not consequences for economy/materiel, for example if the unit is going to use particularly valuable equipment. It is up to the individual unit to choose the assessment criteria for this column.

**Risk = Likelihood x Consequence**

Please calculate the risk value for "Human", "Environment" and, if chosen, "Economy/materiel", separately.

**About the column "Comments/status, suggested preventative and corrective measures":**

Measures can impact on both likelihood and consequences. Prioritise measures that can prevent the incident from occurring; in other words, likelihood-reducing measures are to be prioritised above greater emergency preparedness, i.e. consequence-reducing measures.

NTNU	Risk matrix	prepared by	Number	Date	
		HSE Section	HMSRV2604	8 March 2010	
HSE/KS		approved by	Page	Replaces	
	Rector	4 of 4	9 February 2010		

## MATRIX FOR RISK ASSESSMENTS at NTNU

<b>CONSEQUENCE</b>	Extremely serious	E1	E2	E3	E4	E5
	Serious	D1	D2	D3	D4	D5
	Moderate	C1	C2	C3	C4	C5
	Minor	B1	B2	B3	B4	B5
	Not significant	A1	A2	A3	A4	A5
		Very low	Low	Medium	High	Very high
		<b>LIKELIHOOD</b>				

Principle for acceptance criteria. Explanation of the colours used in the risk matrix.

Colour	Description
Red	Unacceptable risk. Measures must be taken to reduce the risk.
Yellow	Assessment range. Measures must be considered.
Green	Acceptable risk Measures can be considered based on other considerations.



## **Appendix B**

# **Process flow diagram of the Fischer-Tropsch reactor system**

Figure B.1 shows the process flow diagram of the Fischer-Tropsch reactor system used for the activity and selectivity measurements. The figure is adopted from the manual of the rig<sup>[27]</sup>.

APPENDIX B. PROCESS FLOW DIAGRAM OF THE FISCHER-TROPSCH REACTOR SYSTEM

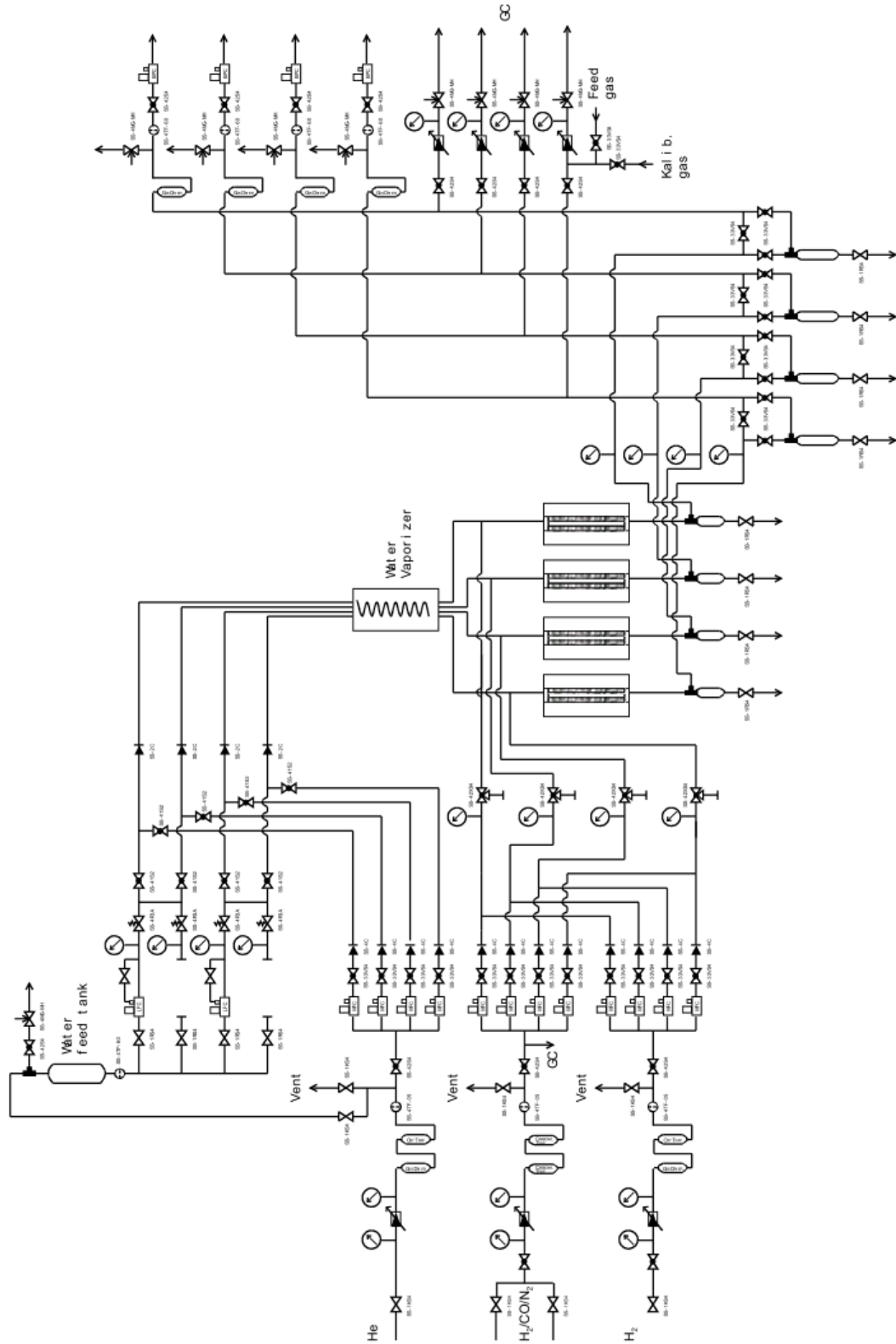


Figure B.1: Flow diagram of the Fischer-Tropsch rig used for the activity and selectivity measurements. Adopted from Myrstad.



# Appendix C

## Chemical calculations for catalyst preparations

### C.1 Amount of chemicals required for preparation of 20Fe2Cu5K

This section shows an example of the calculations prior to the preparation of catalyst 20Fe2Cu5K. Every catalyst was prepared following the same set of equations as shown here. The calculations were conducted with the desire to prepare a catalyst containing iron with a weight fraction of 20%, an amount of copper at 2/100 ratio to iron, and potassium at a 5/100 ratio to iron. The numbers in Tables C.1 and C.2 were used as basis for the calculations. Table C.1 lists the molecular weights of the involving metals, nitrates, and water, and Table C.2 shows the weight fraction of the metals and water in the nitrates used in the preparation.

Table C.1: Molecular weights of the involving metals and their corresponding nitrates, as well as water.

Species	$M_m$ [g/mol]
Fe	55.85
Cu	63.55
K	39.10
$\text{Fe}(\text{NO}_3)_3 \cdot 9\text{H}_2\text{O}$	404.06
$\text{Cu}(\text{NO}_3)_2 \cdot 3\text{H}_2\text{O}$	241.63
$\text{KNO}_3$	101.11
$\text{H}_2\text{O}$	18.02

Table C.2: Weight fractions of the involving metals and water in the left column in the different nitrates in the top row.

$\omega_i$	$\text{Fe}(\text{NO}_3)_3 \cdot 9\text{H}_2\text{O}$	$\text{Cu}(\text{NO}_3)_2 \cdot 3\text{H}_2\text{O}$	$\text{KNO}_3$
<b>Fe</b>	0.1382	-	-
<b>Cu</b>	-	0.2630	-
<b>K</b>	-	-	0.3867
<b>H<sub>2</sub>O</b>	0.4014	0.2237	-

Equation C.1 shows an expression for the desired weight fraction of iron in the finished catalyst.

$$\omega_{\text{Fe}} = \frac{m_{\text{Fe}}}{m_{\text{Fe}} + m_{\text{Al}_2\text{O}_3} + m_{\text{Cu}} + m_{\text{K}}} = 0.20 \quad (\text{C.1})$$

Trying first to find an expression for  $m_{\text{Cu}}$ .

$$n_{\text{Fe}} = \frac{m_{\text{Fe}}}{M_{\text{Fe}}} \quad (\text{C.2})$$

$$n_{\text{Cu}} = \frac{2}{100} \cdot n_{\text{Fe}} \quad (\text{C.3})$$

$$m_{\text{Cu}} = M_{\text{Cu}} \cdot n_{\text{Cu}} \quad (\text{C.4})$$

By combining Equations C.2-C.4, an expression for  $m_{\text{Cu}}$  containing  $m_{\text{Fe}}$  is obtained.

$$m_{\text{Cu}} = M_{\text{Cu}} \cdot \frac{2}{100} \cdot \frac{m_{\text{Fe}}}{M_{\text{Fe}}} \quad (\text{C.5})$$

Now doing the same to get an expression for  $m_{\text{K}}$ .

$$n_{\text{K}} = \frac{5}{100} \cdot n_{\text{Fe}} \quad (\text{C.6})$$

$$m_{\text{K}} = M_{\text{K}} \cdot n_{\text{K}} \quad (\text{C.7})$$

$$m_{\text{K}} = M_{\text{K}} \cdot \frac{5}{100} \cdot \frac{m_{\text{Fe}}}{M_{\text{Fe}}} \quad (\text{C.8})$$

Inserting Equations C.5 and C.8 in Equation C.1 and rearranging, the required expression is obtained.

$$\frac{m_{\text{Fe}}}{m_{\text{Fe}} + m_{\text{Al}_2\text{O}_3} + M_{\text{Cu}} \cdot \frac{2}{100} \cdot \frac{m_{\text{Fe}}}{M_{\text{Fe}}} + M_{\text{K}} \cdot \frac{5}{100} \cdot \frac{m_{\text{Fe}}}{M_{\text{Fe}}}} = 0.20 \quad (\text{C.9})$$

$$\frac{1}{1 + \frac{m_{\text{Al}_2\text{O}_3}}{m_{\text{Fe}}} + \frac{2}{100} \cdot \frac{M_{\text{Cu}}}{M_{\text{Fe}}} + \frac{5}{100} \cdot \frac{M_{\text{K}}}{M_{\text{Fe}}}} = 0.20 \quad (\text{C.10})$$

$$\frac{1}{0.20} = 1 + \frac{m_{\text{Al}_2\text{O}_3}}{m_{\text{Fe}}} + \frac{2}{100} \cdot \frac{M_{\text{Cu}}}{M_{\text{Fe}}} + \frac{5}{100} \cdot \frac{M_{\text{K}}}{M_{\text{Fe}}} \quad (\text{C.11})$$

$$5 - \left( 1 + \frac{2}{100} \cdot \frac{M_{\text{Cu}}}{M_{\text{Fe}}} + \frac{5}{100} \cdot \frac{M_{\text{K}}}{M_{\text{Fe}}} \right) = \frac{m_{\text{Al}_2\text{O}_3}}{m_{\text{Fe}}} \quad (\text{C.12})$$

$$m_{\text{Fe}} = m_{\text{Al}_2\text{O}_3} \cdot \frac{1}{5 - \left( 1 + \frac{2}{100} \cdot \frac{M_{\text{Cu}}}{M_{\text{Fe}}} + \frac{5}{100} \cdot \frac{M_{\text{K}}}{M_{\text{Fe}}} \right)} \quad (\text{C.13})$$

$$m_{\text{Fe}} = m_{\text{Al}_2\text{O}_3} \cdot \frac{M_{\text{Fe}}}{4 \cdot M_{\text{Fe}} - \frac{2}{100} \cdot M_{\text{Cu}} - \frac{5}{100} \cdot M_{\text{K}}} \quad (\text{C.14})$$

Inserting values for  $M_{\text{Fe}}$ ,  $M_{\text{Cu}}$  and  $M_{\text{K}}$  from Table C.1 yields Equation C.15.

$$m_{\text{Fe}} = 0.2537 \cdot m_{\text{Al}_2\text{O}_3} \quad (\text{C.15})$$

Equation C.15 gives an expression for the amount of iron required as a function of the support mass. Combining Equation C.15 with C.5 and inserting values from Table C.1 yields an expression for the mass of copper.

$$m_{\text{Cu}} = 0.2537 \cdot \frac{2}{100} \cdot \frac{M_{\text{Cu}}}{M_{\text{Fe}}} \cdot m_{\text{Al}_2\text{O}_3} = 0.0058 \cdot m_{\text{Al}_2\text{O}_3} \quad (\text{C.16})$$

Using weight fraction values from Table C.2, the amount of nitrates can be derived.

$$m_{\text{Fe}(\text{NO}_3)_3 \cdot 9\text{H}_2\text{O}} = \frac{m_{\text{Fe}}}{\omega_{\text{Fe}}} = \frac{m_{\text{Fe}}}{0.1382} = \frac{0.2537}{0.1382} \cdot m_{\text{Al}_2\text{O}_3} = 1.8357 \cdot m_{\text{Al}_2\text{O}_3} \quad (\text{C.17})$$

$$m_{\text{Cu}(\text{NO}_3)_2 \cdot 3\text{H}_2\text{O}} = \frac{m_{\text{Cu}}}{\omega_{\text{Cu}}} = \frac{m_{\text{Cu}}}{0.2630} = \frac{0.0058}{0.2630} \cdot m_{\text{Al}_2\text{O}_3} = 0.0221 \cdot m_{\text{Al}_2\text{O}_3} \quad (\text{C.18})$$

Since the incipient wetness method is used, the amount of water in the nitrates needs to be calculated, this is shown in Equations C.19 and C.20.

$$m_{\text{H}_2\text{O,Fe}} = \frac{m_{\text{Fe}(\text{NO}_3)_3 \cdot 9\text{H}_2\text{O}}}{\omega_{\text{H}_2\text{O,Fe}}} = \frac{m_{\text{Fe}(\text{NO}_3)_3 \cdot 9\text{H}_2\text{O}}}{0.4014} \quad (\text{C.19})$$

$$m_{\text{H}_2\text{O,Cu}} = \frac{m_{\text{Cu}(\text{NO}_3)_2 \cdot 3\text{H}_2\text{O}}}{\omega_{\text{H}_2\text{O,Cu}}} = \frac{m_{\text{Cu}(\text{NO}_3)_2 \cdot 3\text{H}_2\text{O}}}{0.2237} \quad (\text{C.20})$$

As iron and copper is coimpregnated, the water content of both their nitrates needs to be accounted for. By subtracting the calculated water content in the nitrates from the amount needed to reach incipient wetness point, the required amount of water is then found, as

shown in Equation C.21.

$$m_{\text{H}_2\text{O}} = m_{\text{H}_2\text{O},iwp} - m_{\text{H}_2\text{O},\text{Fe}} - m_{\text{H}_2\text{O},\text{Cu}} \quad (\text{C.21})$$

At this point the potassium is loaded on the catalyst. Small amounts of the catalyst are lost to the environment, so a new calculation of the potassium loading amount is required. This is done by calculating the weight fraction and subsequent mass of  $\text{Al}_2\text{O}_3$  in the catalyst precursor, as shown in Equations C.22 - C.24. From Equation C.15 the mass of iron in the catalyst precursor is then calculated, and by combining Equations C.6 - C.8 into Equation C.25, the expression for required mass of potassium is derived, in Equation C.26.

$$\omega_{\text{Al}_2\text{O}_3} = \frac{m_{\text{Al}_2\text{O}_3}}{m_{\text{Al}_2\text{O}_3} + m_{\text{Fe}} + m_{\text{Cu}}} \quad (\text{C.22})$$

$$\omega_{\text{Al}_2\text{O}_3} = \frac{m_{\text{Al}_2\text{O}_3}}{m_{\text{Al}_2\text{O}_3} + 0.2537 \cdot m_{\text{Al}_2\text{O}_3} + 0.0058 \cdot m_{\text{Al}_2\text{O}_3}} = \frac{1}{1.2595} = 0.7940 \quad (\text{C.23})$$

$$m_{\text{Al}_2\text{O}_3,cat} = \omega_{\text{Al}_2\text{O}_3} \cdot m_{cat} = 0.7940 \cdot m_{cat} \quad (\text{C.24})$$

$$m_{\text{K}} = 0.2537 \cdot \frac{5}{100} \cdot \frac{M_{\text{K}}}{M_{\text{Fe}}} \cdot m_{\text{Al}_2\text{O}_3} = 0.0089 \cdot m_{\text{Al}_2\text{O}_3} \quad (\text{C.25})$$

$$m_{\text{K}} = 0.0089 \cdot 0.7940 \cdot m_{cat} = 0.0071 \cdot m_{cat} \quad (\text{C.26})$$

Using the value of weight fraction from Table C.2, the amount of potassium nitrate can be calculated, as in Equation C.27.

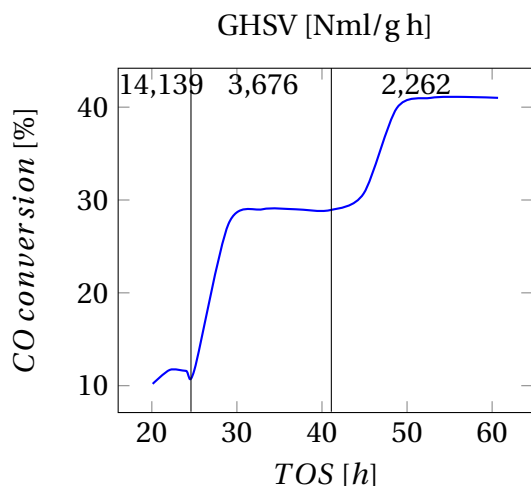
$$m_{\text{KNO}_3} = \frac{m_{\text{K}}}{\omega_{\text{K}}} = \frac{m_{\text{K}}}{0.3867} \quad (\text{C.27})$$

Since potassium nitrate does not contain water, the amount of water needed to reach incipient wetness point is not influenced.

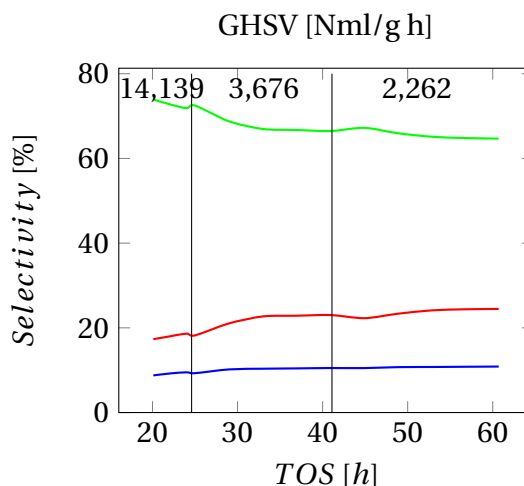
# Appendix D

## Reproduced activity and selectivity measurements

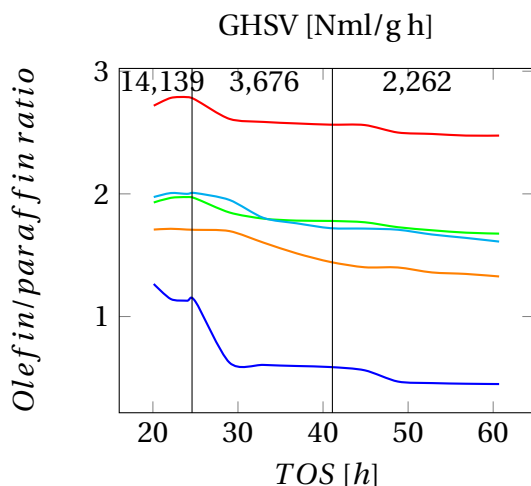
The reproduced activity and selectivity measurements are shown in this appendix. Two of the measurements, shown in Figure D.1 and D.2, were conducted in order to see if the results could be reproduced. Those involved the two experiments run with catalysts 20Fe5K and 20Fe2Cu5K reduced in hydrogen. The reproduced measurements showed similar results as its original measurements, and are therefore not mentioned in great detail in the thesis. The two other measurements, depicted in Figures D.3 and D.4 are reproduced measurements of the two run activated by syngas. This were also the catalysts 20Fe5K and 20Fe2Cu5K. These results were reproduced due to suspicions of deactivation of the catalysts in the original experiments. However, the reproduced experiments were even less active than the ones originally tested.



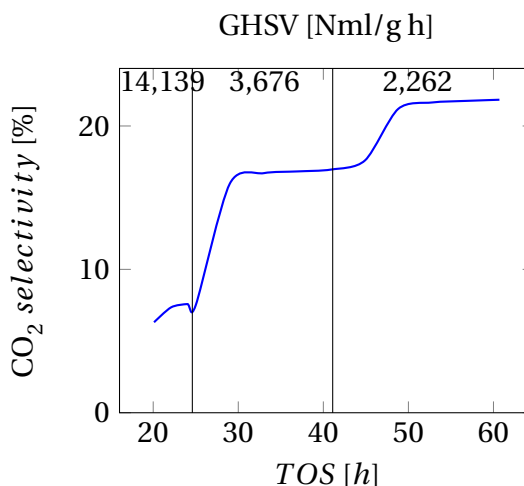
(a) CO conversion as a function of time on stream with GHSV values of 14,139, 3,676 and 2,262 Ncm<sup>3</sup>/g h separated by vertical lines



(b) Selectivities of CO<sub>2</sub>-free CH<sub>4</sub>, C<sub>2</sub>-C<sub>4</sub> and C<sub>5</sub>+ as a function of time on stream with GHSV values of 14,139, 3,676 and 2,262 Ncm<sup>3</sup>/g h separated by vertical lines. (Blue) CH<sub>4</sub>, (Red) C<sub>2</sub>-C<sub>4</sub>, (Green) C<sub>5</sub>+

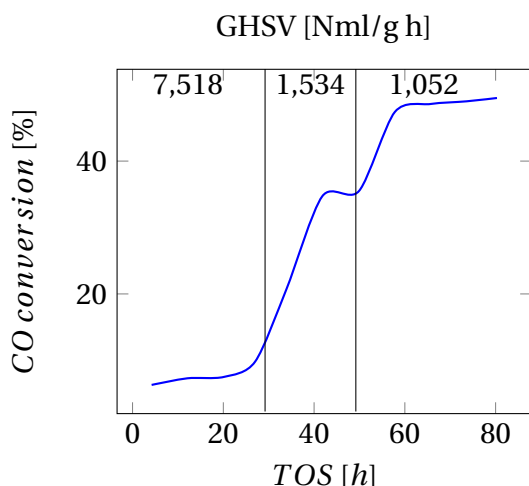


(c) Olefin/paraffin ratio as a function of time on stream with GHSV values of 14,139, 3,676 and 2,262 Ncm<sup>3</sup>/g h separated by vertical lines. (Blue) C<sub>2</sub>, (Red) C<sub>3</sub>, (Green) C<sub>4</sub>, (Cyan) C<sub>5</sub>, (Orange) C<sub>6</sub>.

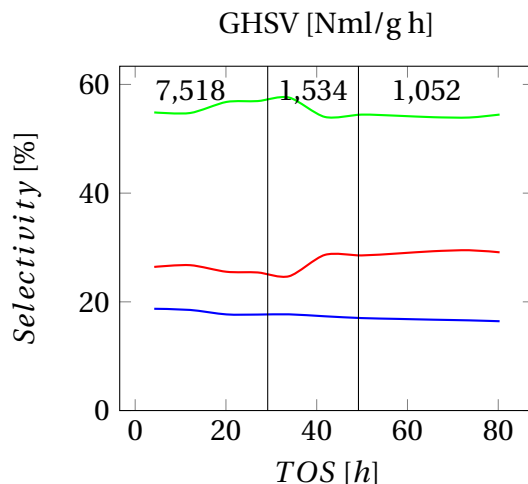


(d) CO<sub>2</sub> selectivity as a function of time on stream with GHSV values of 14,139, 3,676 and 2,262 Ncm<sup>3</sup>/g h separated by vertical lines

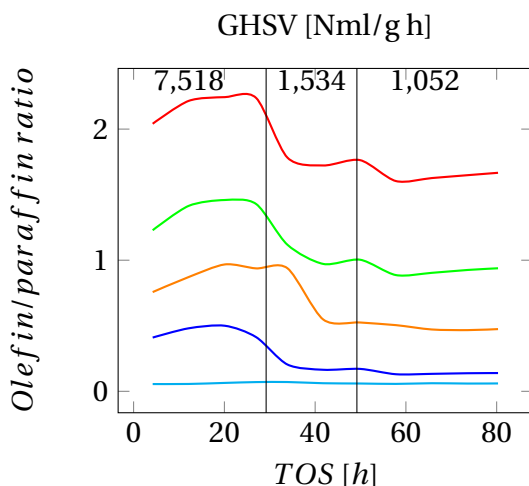
Figure D.1: Activity and selectivity plots of reproduced experiments of the 20Fe5K catalyst at 20 bar and 230 °C reduced with hydrogen



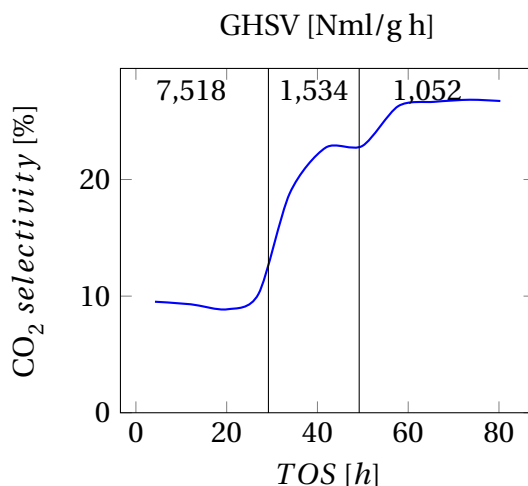
(a) CO conversion as a function of time on stream with GHSV values of 7518, 1534 and 1052 Ncm<sup>3</sup>/g h separated by vertical lines



(b) Selectivities of CO<sub>2</sub>-free CH<sub>4</sub>, C<sub>2</sub>-C<sub>4</sub> and C<sub>5</sub>+ as a function of time on stream with GHSV values of 7518, 1534 and 1052 Ncm<sup>3</sup>/g h separated by vertical lines. (Blue) CH<sub>4</sub>, (Red) C<sub>2</sub>-C<sub>4</sub>, (Green) C<sub>5</sub>+



(c) Olefin/paraffin ratio as a function of time on stream with GHSV values of 7518, 1534 and 1052 Ncm<sup>3</sup>/g h separated by vertical lines. (Blue) C<sub>2</sub>, (Red) C<sub>3</sub>, (Green) C<sub>4</sub>, (Cyan) C<sub>5</sub>, (Orange) C<sub>6</sub>.



(d) CO<sub>2</sub> selectivity as a function of time on stream with GHSV values of 7517 and 1534 and 1052 Ncm<sup>3</sup>/g h separated by vertical lines

Figure D.2: Activity and selectivity plots of reproduced experiments of the 20Fe2Cu5K catalyst at 20 bar and 230 °C reduced with hydrogen

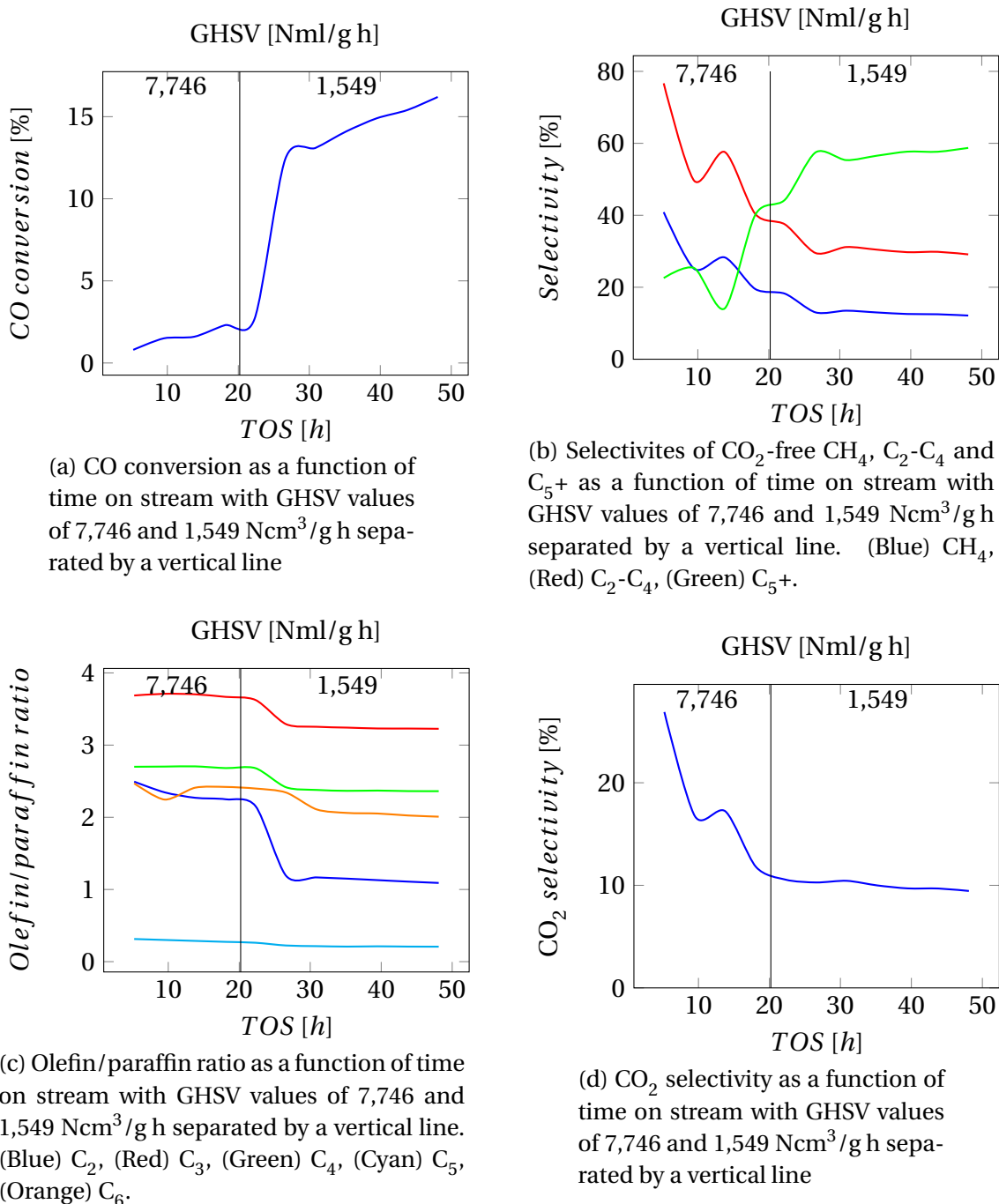
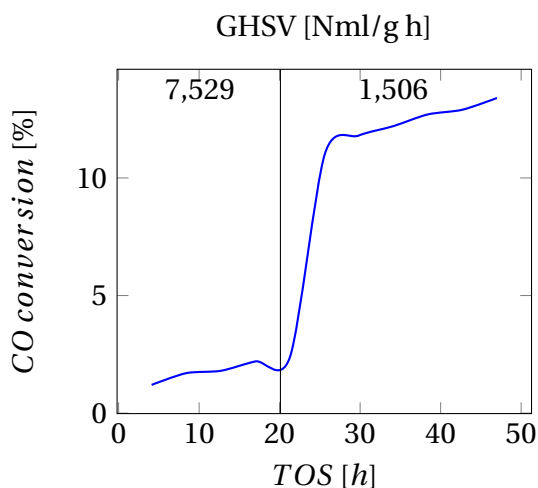
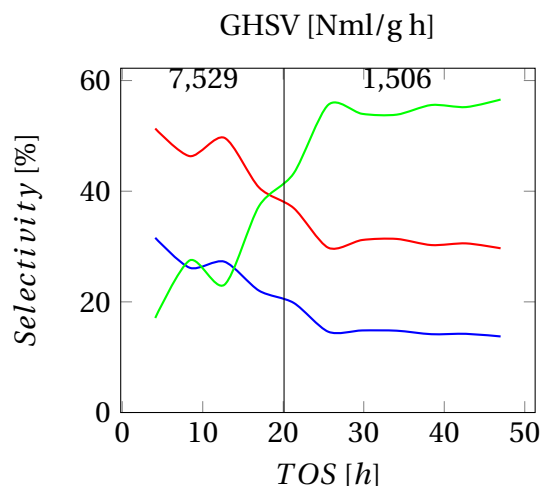


Figure D.3: Activity and selectivity plots of reproduced experiments of the 20Fe5K catalyst at 20 bar and 230 °C reduced with syngas

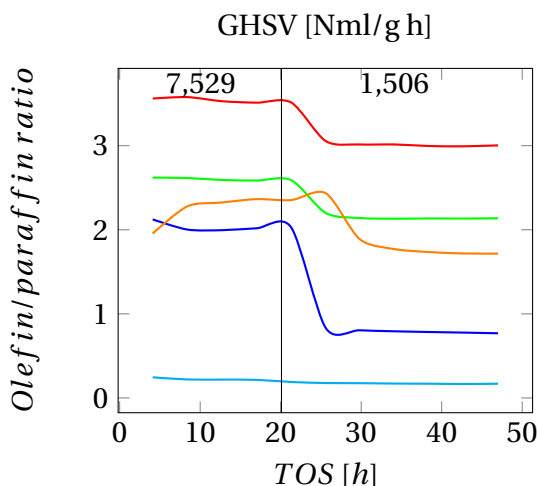




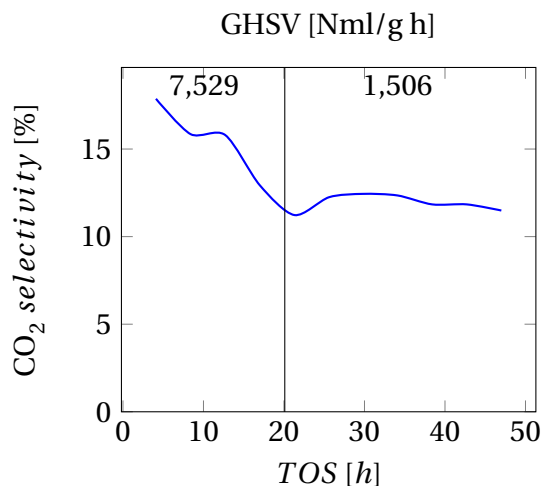
(a) CO conversion as a function of time on stream with GHSV values of 7,529 and 1,506 Ncm<sup>3</sup>/g h separated by a vertical line



(b) Selectivities of CO<sub>2</sub>-free CH<sub>4</sub>, C<sub>2</sub>-C<sub>4</sub> and C<sub>5</sub>+ as a function of time on stream with GHSV values of 7,529 and 1,506 Ncm<sup>3</sup>/g h separated by a vertical line. (Blue) CH<sub>4</sub>, (Red) C<sub>2</sub>-C<sub>4</sub>, (Green) C<sub>5</sub>+



(c) Olefin/paraffin ratio as a function of time on stream with GHSV values of 7,529 and 1,506 Ncm<sup>3</sup>/g h separated by a vertical line. (Blue) C<sub>2</sub>, (Red) C<sub>3</sub>, (Green) C<sub>4</sub>, (Cyan) C<sub>5</sub>, (Orange) C<sub>6</sub>.



(d) CO<sub>2</sub> selectivity as a function of time on stream with GHSV values of 7,529 and 1,506 Ncm<sup>3</sup>/g h separated by a vertical line

Figure D.4: Activity and selectivity plots of reproduced experiments of the 20Fe2Cu5K catalyst at 20 bar and 230 °C reduced with syngas